ANTIOXIDANTS & REDOX SIGNALING
Volume 22, Number 3, 2015

DOI: 10.1089/ars.2013.5818

Discoveries

ORIGINAL RESEARCH COMMUNICATION

The Angiotensin-Converting Enzyme 2/Angiotensin (1–7)/Mas Axis Protects Against Lung Fibroblast Migration and Lung Fibrosis by Inhibiting the NOX4-Derived ROS-Mediated RhoA/Rho Kinase Pathway

Ying Meng,[1] Ting Li,[1] Gao-su Zhou,[2] Yan Chen,[1] Chang-Hui Yu,[1] Miao-Xia Pang,[1] Wei Li,[1] Yang Li,[3] Wen-Yong Zhang,[3] and Xu Li[3,4]

Abstract

Reactive oxygen species (ROS) generated by NADPH oxidase-4 (NOX4) have been shown to initiate lung fibrosis. The migration of lung fibroblasts to the injured area is a crucial early step in lung fibrosis. The angiotensin-converting enzyme 2 (ACE2)/angiotensin (1–7) [Ang(1–7)]/Mas axis, which counteracts the ACE/angiotensin II (AngII)/angiotensin II type 1 receptor (AT1R) axis, has been shown to attenuate pulmonary fibrosis. Nevertheless, the exact molecular mechanism remains unclear. ***Aims:*** To investigate the different effects of the two axes of the renin-angiotensin system (RAS) on lung fibroblast migration and extracellular matrix accumulation by regulating the NOX4-derived ROS-mediated RhoA/Rho kinase (Rock) pathway. ***Results:*** *In vitro*, AngII significantly increased the NOX4 level and ROS production in lung fibroblasts, which stimulated cell migration and α-collagen I synthesis through the RhoA/Rock pathway. These effects were attenuated by *N*-acetylcysteine (NAC), diphenylene iodonium, and NOX4 RNA interference. Moreover, Ang(1–7) and lentivirus-mediated ACE2 (lentiACE2) suppressed AngII-induced migration and α-collagen I synthesis by inhibiting the NOX4-derived ROS-mediated RhoA/Rock pathway. However, Ang(1–7) alone exerted analogous effects on AngII. *In vivo*, constant infusion with Ang(1–7) or intratracheal instillation with lenti-ACE2 shifted the RAS balance toward the ACE2/Ang(1–7)/Mas axis, alleviated bleomycin-induced lung fibrosis, and inhibited the RhoA/Rock pathway by reducing NOX4-derived ROS. ***Innovation*:** This study suggests that the ACE2/Ang(1–7)/Mas axis may be targeted by novel pharmacological antioxidant strategies to treat lung fibrosis induced by AngII-mediated ROS. ***Conclusion:*** The ACE2/Ang(1–7)/Mas axis protects against lung fibroblast migration and lung fibrosis by inhibiting the NOX4-derived ROS-mediated RhoA/Rock pathway. *Antioxid. Redox Signal*. 22, 241–258.

Introduction

PULMONARY FIBROSIS is a frequent response to lung injuries (45). Lung fibroblasts play a key role in the initiation and progression of pulmonary fibrosis *via* the proliferation, migration, and synthesis of extracellular matrix (ECM) components (14, 43). Pulmonary fibroblast migration is essential for fibrosis, because these cells migrate to wounded areas, accumulate, and then secrete ECM proteins (43, 44). Hence, inhibition of pulmonary fibroblast migration to the wounded area may be a promising treatment for pulmonary fibrosis.

Recently, much research has focused on the effects of oxidative stress on the pathogenesis of pulmonary fibrosis (10, 15, 20). Oxidative stress is defined as an imbalance between the generation of reactive oxygen species (ROS) in excess of the capacity of cells/tissues to detoxify or scavenge these molecules. ROS generation plays a relevant role in lung fibrosis, and recent studies suggest that NADPH oxidases

[1]Department of Respiratory Diseases, Nanfang Hospital, the Southern Medical University, Guangzhou, China.
[2]Department of Emergency Medicine, the Military General Hospital of Beijing PLA, Beijing, China.
Departments of [3]Emergency Medicine and [4]Hepatology, Nanfang Hospital, the Southern Medical University, Guangzhou, China.

Innovation

The angiotensin-converting enzyme 2 (ACE2)/Ang(1–7)/Mas axis, which counteracts the activity of the ACE/AngII/AT1R axis, has been shown to protect against pulmonary fibrosis. Nevertheless, the exact molecular mechanism remains unclear. For the first time, we have demonstrated that AngII induces lung fibroblast migration and α-collagen I synthesis by upregulating the NADPH oxidase-4 (NOX4)-derived, ROS-mediated RhoA/Rock pathway. Ang(1–7) and lentiACE2 prevented AngII-induced lung fibroblast migration and bleomycin-induced lung fibrosis by inhibiting the NOX4-derived, ROS-mediated RhoA/Rock pathway. This study suggests that the ACE2/Ang(1–7)/Mas axis should be targeted in novel pharmacological antioxidant strategies for lung fibrosis induced by AngII-mediated ROS.

(NOXs) are key sources of ROS in the fibrotic lung (7, 27). NOXs include seven members, which have been identified as NOX1-5 and Duox-1 and – 2. Each NOX catalyzes the reduction of molecular oxygen (O_2) to superoxide (O_2^-) (6). Various NOX homologs expressed in different pulmonary cell types contribute to lung fibrosis (16). In recent years, the key roles of NOXs (specifically NOX4) in mediating fibroblast functions during the lung fibrosis process have been stressed. Specifically, the mRNA level of nonphagocytic NOX4 was highest among NADPH family isoforms in lung fibroblasts isolated from human lung tissue with idiopathic pulmonary fibrosis (IPF) (1) or stimulated with transforming growth factor β (TGFβ) (17). Furthermore, NOX4-dependent generation of ROS (especially hydrogen peroxide [H_2O_2]) was found to be required for TGFβ-induced ECM generation and platelet-derived growth factor (PDGF)-induced migration of lung fibroblasts (1, 17); however, deficiencies in NOX4 or *N*-acetylcysteine (NAC), a scavenger of ROS, protected against bleomycin (BLM)-induced pulmonary fibrosis (17, 40) and PDGF-induced lung fibroblast migration (1). Hence, NOX4 is a promising target for the treatment of lung fibrosis.

In addition, recent studies have shown that ROS caused the activation of RhoA (21), the small GTPase that regulates cell migration (17) and α-collagen I secretion (21). Furthermore, NOX-derived ROS generation led to vascular smooth muscle cell (VSMC) migration by upregulating the RhoA/Rho kinase (Rock) pathway (26, 31). However, it remains unclear whether RhoA is activated by NOX4-derived ROS in the initiation of lung fibroblast migration.

A growing body of evidence indicates that angiotensin II (AngII), a key bioactive peptide of the renin-angiotensin system (RAS) that is generated from angiotensin I (AngI) by angiotensin-converting enzyme (ACE), is an important profibrotic mediator which induces normal lung fibroblast migration (20) and collagen synthesis (28, 36) by binding to the AngII type 1 receptor (AT1R). Recently, the activation of the NOX-dependent generation of superoxide induced by AngII has emerged as a critical pathogenic factor in the development of pulmonary fibrosis (53). However, the majority of studies have primarily focused on the ECM deposition initiated by AngII-induced oxidative stress during the lung fibrosis process (53), and the role of AngII-induced NOX-derived ROS in lung fibroblast migration has not been reported. In VSMCs, aldosterone/AngII stimulated cell migration by increasing the NOX-derived generation of ROS, which subsequently upregulated the RhoA/Rock pathway (31). Thus, we hypothesized that AngII induces pulmonary fibroblast migration *via* the NOX4-derived ROS-mediated RhoA/Rock pathway.

In contrast, ACE2, a homolog of ACE, is a recently discovered enzyme that catalyzes angiotensin II into angiotensin(1–7) [Ang(1–7)]. The ACE2/Ang(1–7)/Mas axis, which consists of new RAS components that counter-regulate the ACE/AngII/AT1R axis, protects against lung fibrosis. Treatment with Ang(1–7) or ACE2 improved BLM-induced lung fibrosis (38, 41), whereas ACE2 depletion exacerbated collagen deposition in mice (38). Nevertheless, the exact molecular mechanism by which the ACE2/Ang(1–7)/Mas axis protects against lung fibrosis remains incompletely understood. The effects of ACE2/Ang(1–7) on AngII-induced lung fibroblast migration remain unclear. Interestingly, emerging evidence suggests that ACE2 (11, 51, 59) and Ang(1–7) (19, 32) possess antioxidant effects which protect against injuries induced by NOX-mediated oxidative stress in the kidney (32), the brain (10, 19, 51), and the cardiovascular system (59). A potential mechanism is that ACE2 catalyzes the conversion of AngII into Ang(1–7), leading to the attenuation of oxidative stress. Furthermore, Ang(1–7) blocked AngII-stimulated Rock phosphorylation through Mas receptor activation in rat hearts *in vivo* (13) and inhibited AngII-induced VSMC migration (55). ACE2 overexpression significantly attenuated AngII-induced migration in VSMCs *via* the downregulation of AngII-induced ROS-NF-κB signaling pathways (54). A reduction in ACE2 expression in pulmonary artery smooth muscle cells by RNA interference significantly enhanced cell migration induced by hypoxia (56). Therefore, we hypothesized that the ACE2/Ang(1–7)/Mas axis protects against lung fibroblast migration and ECM accumulation by suppressing the NOX4-derived ROS-mediated RhoA/Rock pathway.

To test the hypothesis that the ACE2/Ang(1–7)/Mas axis antagonizes the ACE/AngII/AT1R axis-mediated pathophysiological activation of processes leading to lung fibrosis, we investigated the different effects of the two RAS axes on lung fibroblast migration and ECM accumulation by regulating the NOX4/ROS/RhoA/Rock pathway. For the first time, we demonstrated that AngII induced lung fibroblast migration and α-collagen I synthesis by upregulating the NOX4/ROS/RhoA/Rock pathway. In contrast, Ang(1–7) and ACE2 overexpression prevented AngII-induced lung fibroblast migration and BLM-induced lung fibrosis by inhibiting the NOX4/ROS/RhoA/Rock pathway.

Results

AngII induced migration and α-collagen I synthesis in lung fibroblasts

We examined the effect of AngII (10^{-9}–10^{-5} *M*) on rat primary lung fibroblast migration and α-collagen I synthesis. As Figure 1 shows, AngII increased lung fibroblast migration and α-collagen I and α-smooth actin (α-sma) production, and these effects peaked at 10^{-7} m*M* of AngII (Fig. 1A–C).

AngII increased NOX4 expression and ROS generation in lung fibroblasts

To determine the NOX isoform changes in rat lung fibroblasts stimulated with AngII, we measured NOX protein and

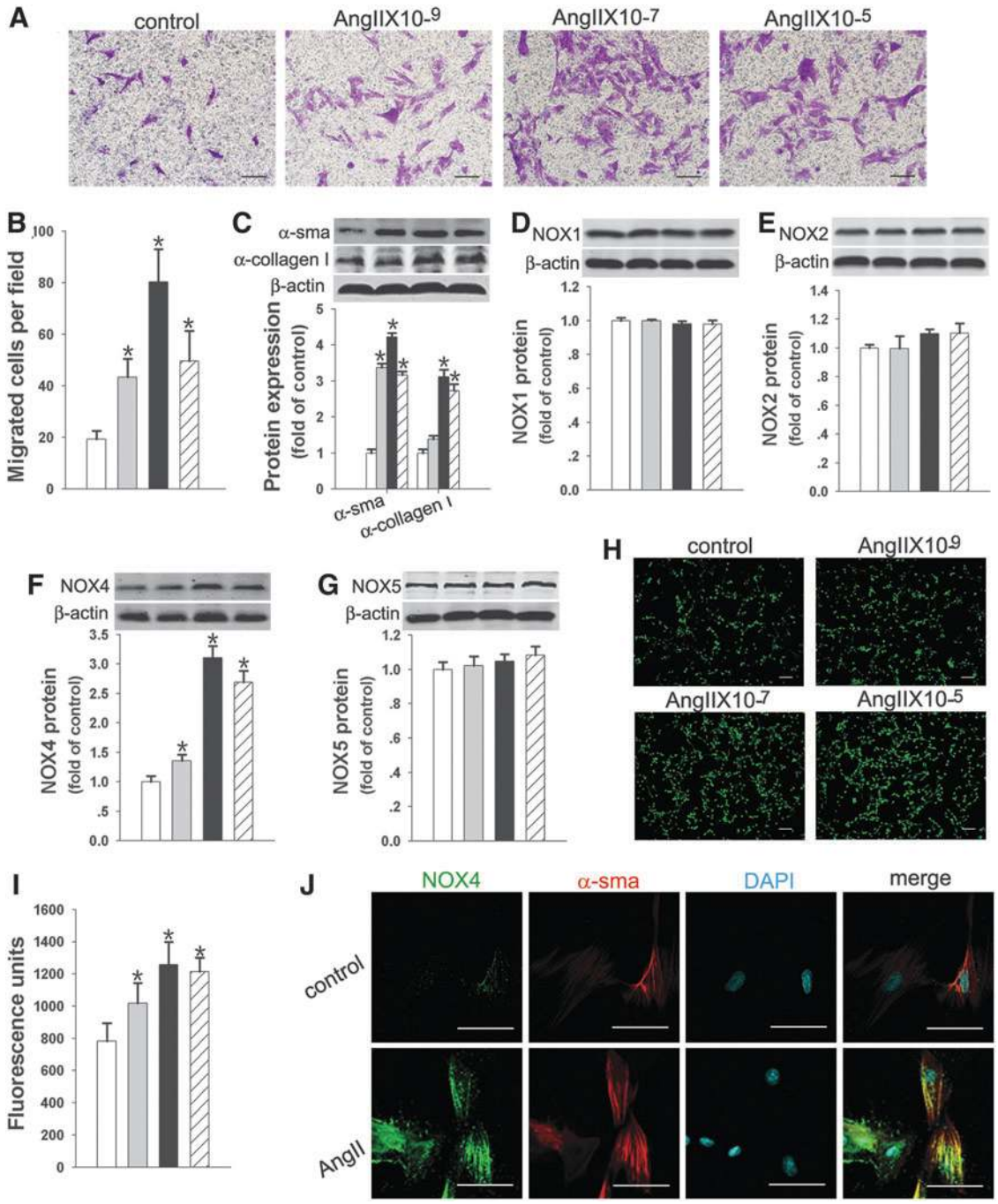

FIG. 1. AngII induced migration, α-collagen I synthesis, and ROS production in lung fibroblasts. Serum-deprived fibroblasts were incubated with varying concentrations of AngII (10^{-9}, 10^{-7}, and 10^{-5} *M*) for 12 h (for migration) or 24 h. **(A)** Cell migration assays were performed using Corning cell culture inserts. Representative photomicrographs of lung fibroblasts subjected to crystal violet staining. **(B)** Measurement of the migrated cell counts. **(C)** Western blot analysis of α-sma and α-collagen I proteins. **(D–G)** Western blot analysis of NOXs (NOX1, 2, 4, and 5) protein. **(H)** Representative photomicrographs of cells subjected to DCF-DA treatment. **(I)** Measurement of DCF-DA fluorescence intensity. **(J)** Dual immunofluorescence for NOX4 (*green*) and α-sma (*red*). Nuclei are stained with DAPI (*blue*). Images are representative of three separate experiments. Data are the means ± SD of three independent experiments. Scale bar = 200 μm. $^{*}p < 0.05$ *versus* control. α-sma, α-smooth actin; DCF-DA, 2,7-dichlorofluorescein diacetate; NOX, NADPH oxidase; ROS, reactive oxygen species.

mRNA levels. The gene or protein level of the nonphagocytic NOX4 was significantly upregulated in lung fibroblasts treated with AngII (10^{-9}–10^{-5} *M*); however, the gene or protein level of other NOX isoforms (phagocytic NOX2, nonphagocytic NOX1 and NOX5) was slightly increased, and the difference was not statistically significant (Fig. 1D–G and Supplementary Fig. S1A; Supplementary Data are available online at www.liebertpub.com/ars). Rac1 is a cytosolic subunit that is essential for activating NOX isoforms. The role of Rac1 in AngII-induced NOX4 activation in lung

fibroblasts remains unknown. A glutathione S-transferase (GST) pull-down assay showed that AngII treatment increased active Rac1 protein levels in lung fibroblasts (Supplementary Fig. S1B). Coimmunoprecipitation assay suggested that interactions between NOX4 and Rac1 were significantly enhanced in lung fibroblasts after AngII stimulation (Supplementary Fig. S1C). Furthermore, the Rac1 inhibitor Ehop significantly reduced AngII-induced protein levels of NOX4 and α-collagen I. Hence, Rac1 plays a key role in AngII-induced NOX4 activation and the consequent α-collagen I synthesis. In addition, AngII stimulation resulted in a rapid increase of ROS production that peaked at 10^{-7} *M* (Fig. 1H, I). Finally, double-label fluorescent immunohistochemistry showed that the NOX4 protein level increased and intensely co-localized with α-sma in lung fibroblasts after treatment with 10^{-7} *M* AngII (yellow in the merged panel in Fig. 1J). Consequently, there is a potential link between AngII-induced NOX4 and lung fibroblast migration and collagen production.

NOX4-generated ROS were required for AngII-induced migration and α-collagen I synthesis in lung fibroblasts

NOX4 upregulation correlates with the migration and α-collagen I synthesis in AngII-stimulated lung fibroblasts. Therefore, we investigated whether AngII-induced lung fibroblast migration and α-collagen I synthesis were mediated by NOX4-generated ROS. The results showed that the increase in ROS and the overproduction of H_2O_2 in AngII-stimulated lung fibroblasts were abolished by pretreatment with the NADPH inhibitor diphenylene iodonium (DPI) (Fig. 2A–C) or NOX4

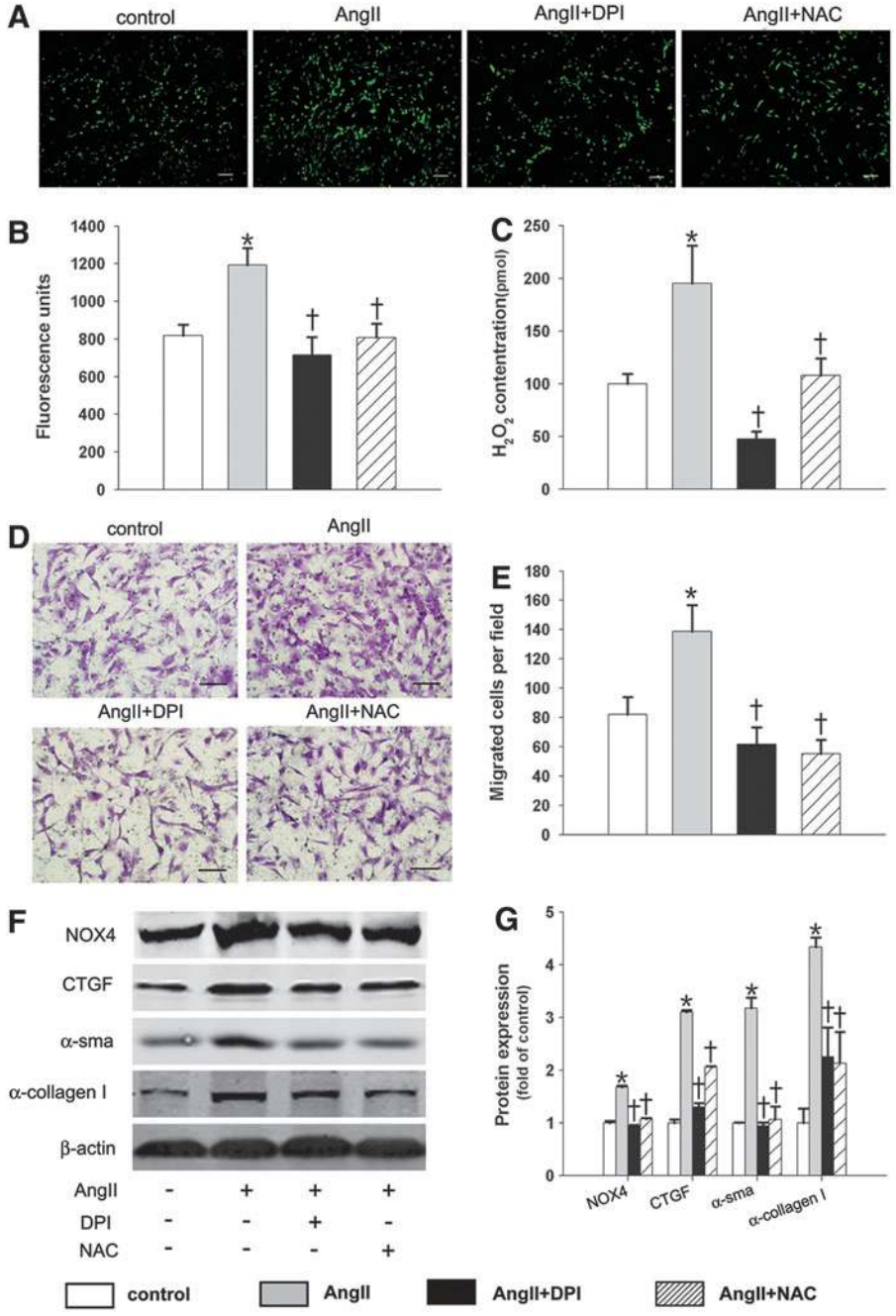

FIG. 2. NOX-derived ROS mediated AngII-induced lung fibroblast migration and α-collagen I synthesis. Fibroblasts were pretreated with DPI (10^{-5} *M*) or NAC (10^{-3} *M*) for 1 h before stimulation with AngII (10^{-7} *M*) as indicated for 12 h (for migration) or 24 h. **(A, B)** Intracellular ROS production was quantified by measuring DCF-DA. **(C)** The H_2O_2 concentration was detected. **(D, E)** Lung fibroblast cell migration assays. **(F, G)** Western blot analysis of NOX4, CTGF, α-SMA, and α-collagen I protein levels. Data are the means ± SD of three independent experiments. Scale bar = 200 μm. $^{*}p < 0.05$ *versus* control; $^{\dagger}p < 0.05$ *versus* AngII. DPI, diphenylene iodonium; H_2O_2, hydrogen peroxide; NAC, *N*-acetylcysteine.

small-interfering RNA (siRNA) (Fig. 3A–C). Moreover, pretreatment with the ROS scavenger NAC, DPI, or NOX4 siRNA suppressed the increases in AngII-induced cell migration, connective tissue growth factor (CTGF), α-sma, and α-collagen I protein levels (Figs. 2D–G and 3D–G). Overall, these results suggest that NOX4-dependent ROS mediated the effects of AngII on lung fibroblast migration and α-collagen I composition.

NOX4-derived ROS were required for AngII-induced RhoA/Rock pathway activation in lung fibroblasts

We next investigated the activation of intracellular signaling molecules, such as RhoA (21, 31), by AngII. First, we found that AngII caused rapid increases in the levels of active RhoA, p-moesin protein, and Rock2 mRNA (Fig. 4A–F). Moreover, Y27632, the Rock inhibitor, blocked increases in fibroblast migration and α-collagen I protein in AngII-stimulated cells (Fig. 4G–I). These results suggest that the RhoA/Rock pathway is involved in AngII-induced pro-migratory and pro-fibrotic effects. Next, we found that pretreatment with DPI or NAC significantly inhibited the AngII-induced increase in active RhoA protein, p-moesin protein, and Rock2 mRNA (Fig. 4A–C). Similarly, NOX4 siRNA transfection also suppressed the RhoA/Rock pathway stimulated by AngII (Fig. 4D–F). Collectively, these results confirmed that NOX4-derived ROS mediated the AngII-induced RhoA/Rock pathway.

Ang(1–7) suppressed AngII-induced fibroblast migration and α-collagen I synthesis by inhibiting the NOX4/ROS/RhoA/Rock pathway

Emerging data show that the ACE2/Ang(1–7)/Mas axis counteracts the pro-fibrotic effects of the ACE/AngII/AT1R axis. Therefore, we investigated whether Ang(1–7) interfered with AngII's effects on cell migration and α-collagen I synthesis. As Figure 5 shows, AngII led to significant increases in cell migration (Fig. 5A, B) and α-sma, CTGF, and α-collagen I protein levels (Fig. 5C, D). Ang(1–7) significantly inhibited the AngII effects mentioned earlier, and the inhibitory effects of Ang(1–7) were reversed by the addition of a Mas receptor antagonist, A779 (Fig. 5A–D).

Next, we investigated the direct effect of Ang(1–7) on the AngII-induced TGFβ/NOX4/ROS/RhoA/Rock pathway. As Figure 5E and F shows, TGFβ mRNA and NOX4 protein markedly increased in response to AngII treatment in lung fibroblasts; this response was blocked by Ang(1–7) and the AT1R inhibitor irbesartan. Dihydroethidium fluorescence imaging and H_2O_2 production showed similar increases in

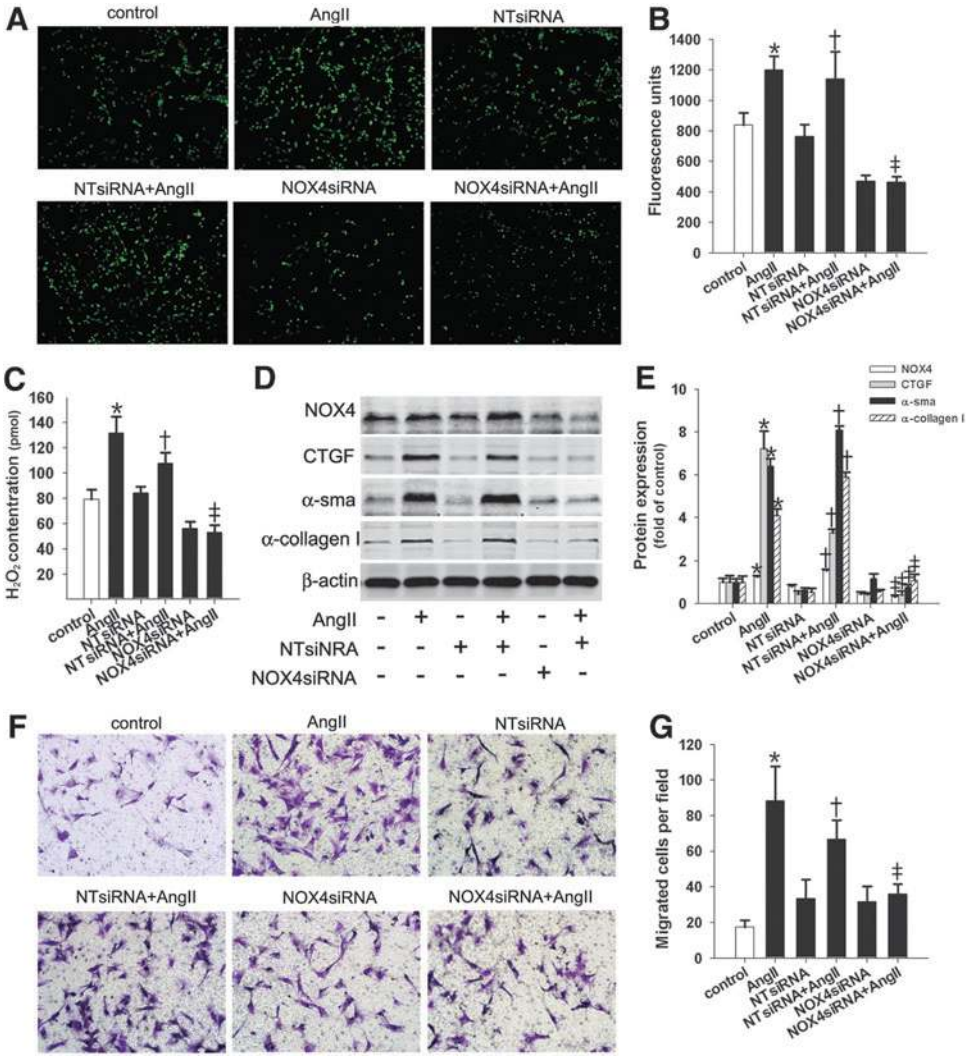

FIG. 3. siRNA targeting NOX4 suppressed AngII-induced lung fibroblast migration and α-collagen synthesis. Lung fibroblasts were transfected with siRNA targeting NOX4 (NOX4 siRNA). Forty-eight hours later, the cells were treated with 10^{-7} *M* of AngII for 12 h (for migration) or 24 h or were left untreated. **(A, B)** Intracellular ROS production was quantified by measuring DCF-DA. **(C)** The H_2O_2 concentration was measured. **(D, E)** Western blot analysis of NOX4, CTGF, α-SMA, and α-collagen I protein expression. **(F, G)** Lung fibroblast cell migration assays. Data are the means ± SD from three independent experiments. Scale bar = 200 μm. $^{*}p < 0.05$ *versus* control; $^{\dagger}p < 0.05$ *versus* NT siRNA; $^{\ddagger}p < 0.05$ *versus* NT siRNA + AngII. siRNA, small-interfering RNA.

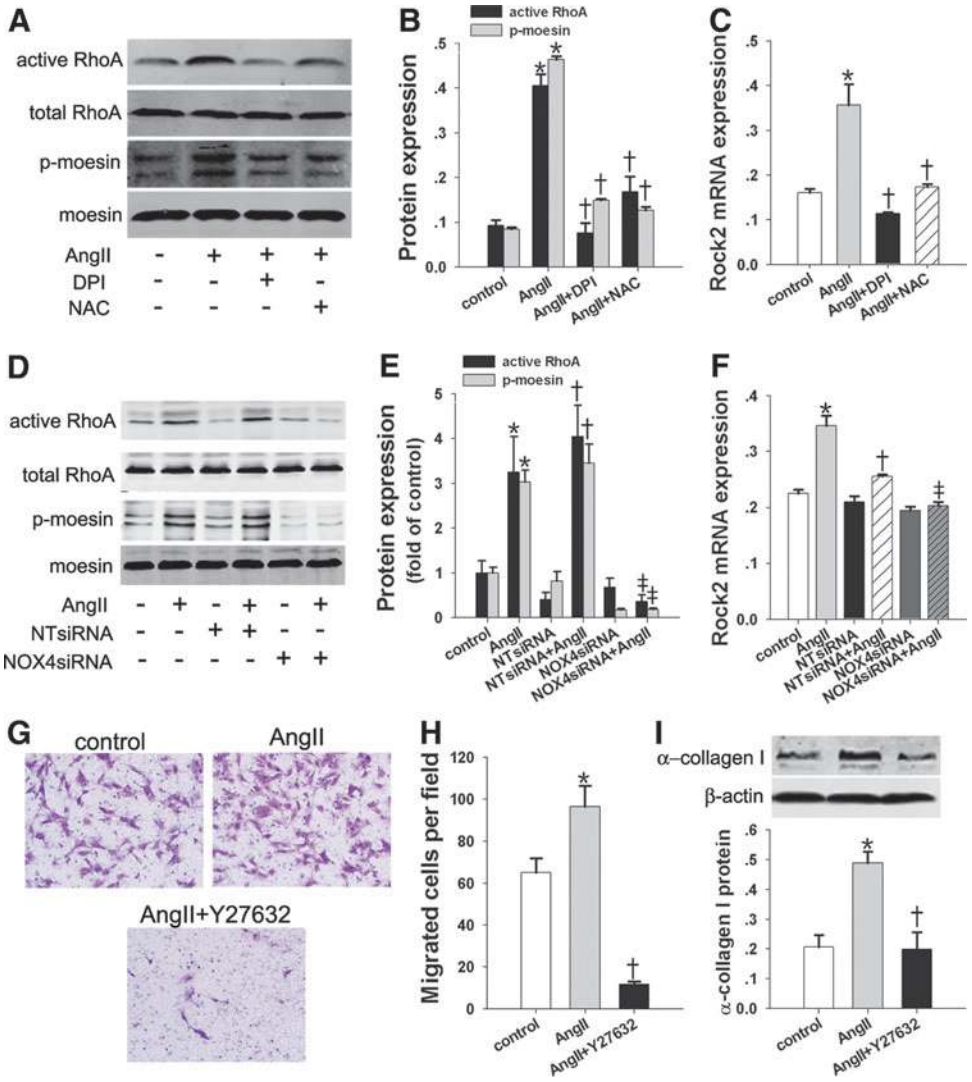

FIG. 4. Inhibition of NOX4 or antioxidant treatment prevented activation of the AngII-induced RhoA/Rock pathway. Cells were pretreated with DPI (10^{-5} *M*) or NAC (10^{-3} *M*) for 1 h or were transfected with NOX4 siRNA before stimulation with AngII (10^{-7} *M*) as indicated for 30 min (for p-moesin) or 24 h. **(A, B)** GTP-loaded RhoA (active RhoA) was determined using the GST pull-down assay with GST-Rhotekin-RBD. p-moesin protein was detected with Western blot. **(C)** The Rock2 mRNA level was measured using real-time PCR. **(D, E)** Active RhoA was determined using the GST pull-down assay; p-moesin protein was detected with Western blot. **(F)** The Rock2 mRNA level was measured with real-time PCR. **(G–I)** Cells were pretreated with Y27632 (10^{-5} *M*) for 1 h before stimulation with AngII (10^{-7} *M*) for 12 h (for migration) or 24 h. **(G, H)** The cell migration assays were used to determine the migration of lung fibroblasts. **(I)** The α-collagen I protein level was detected with Western blot. Data are the means ± SD of three independent experiments. Scale bar = 200 μm. **p* < 0.0 5 *versus* controls; †*p* < 0.0 5 *versus* AngII or NT siRNA; ‡*p* < 0.05 *versus* NT siRNA + AngII. GST, glutathione S-transferase; PCR, polymerase chain reaction; Rock, Rho kinase. To see this illustration in color, the reader is referred to the web version of this article at www.liebertpub.com/ars

AngII that were also abolished by Ang(1–7) and irbesartan (Fig. 5H–J). However, co-incubation with A779 neutralized these effects of Ang(1–7) (Fig. 5F–J). In addition, expression analyses showed that AngII-induced levels of active RhoA, p-moesin protein, and Rock2 mRNA were markedly reduced by Ang(1–7), and the inhibitory effects were reversed by A779 (Fig. 5E–G). These effects of Ang(1–7) were similar to those of irbesartan. The *in vitro* results suggest that AT1R mediates the pro-fibrotic effects of AngII, whereas Mas-dependent signaling is involved in the antioxidative actions of Ang(1–7) on AngII.

Ang(1–7) alone promoted fibroblast migration and α-collagen I synthesis by activating the NOX4/ROS/RhoA/Rock pathway via *the AT1R*

In vitro, Ang(1–7) (10^{-7} *M*) alone promoted lung fibroblast migration and α-collagen I protein expression compared with the control group (Fig. 5A–C and Supplementary Fig. S2A–C), although there were no differences in CTGF and α-sma protein (Fig. 5C, D). These pro-migrated and pro-fibrotic effects were accompanied by increases in TGFβ mRNA, NOX4 protein, ROS production, H_2O_2 production, active

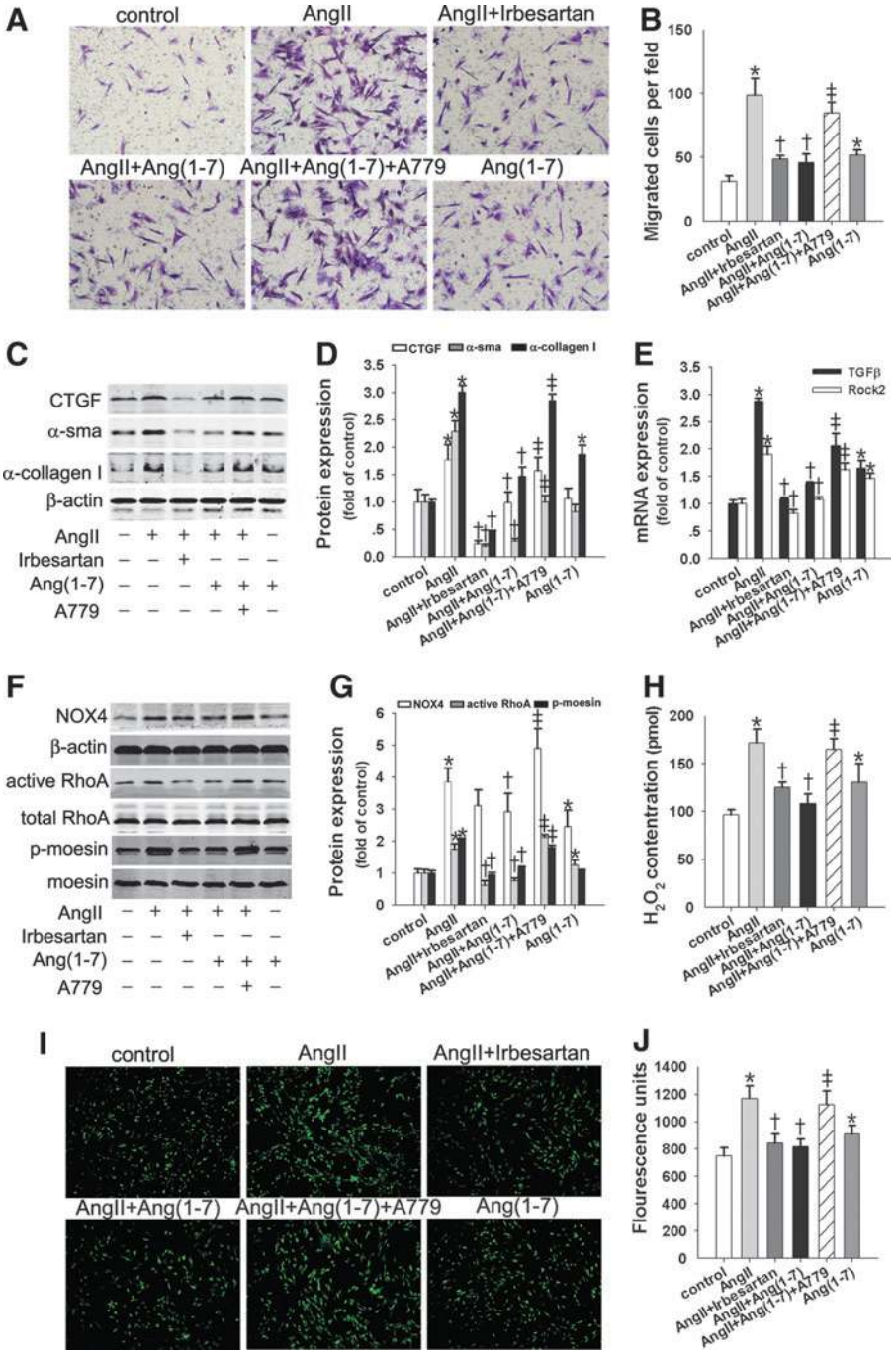

FIG. 5. Ang(1–7) suppressed AngII-induced fibroblast migration and α-collagen I synthesis by inhibiting the NOX4/ROS/RhoA/Rock pathway. Lung fibroblasts were pretreated with irbesartan (10^{-5} *M*) or A779 (10^{-5} *M*) for 1 h before exposure to Ang(1–7) (10^{-7} *M*) or (+) AngII (10^{-7} *M*) for the indicated times. **(A, B)** Lung fibroblast migration assays. **(C, D)** Western blot was performed to measure the CTGF, α-SMA, and α-collagen I protein levels. **(E)** TGFβ and Rock2 mRNA levels were detected with real-time reverse transcription-polymerase chain reaction (RT-PCR). **(F, G)** Active RhoA was determined using the GST pull-down assay; NOX4 and p-moesin protein were detected with Western blot. **(H)** The H_2O_2 concentration was measured. **(I, J)** Intracellular ROS production was quantified by measuring DCF-DA. Data are the means ± SD of three independent experiments. Scale bar = 200 μm. $^{*}p < 0.05$ *versus* controls; $^{\dagger}p < 0.05$ *versus* AngII; $^{\ddagger}p < 0.05$ *versus* AngII + Ang(1–7). TGFβ, transforming growth factor β.

RhoA protein, and Rock2 mRNA (Fig. 5E–J and Supplementary Fig. S2C, D). *In vivo*, continuous infusion with Ang(1–7) significantly enhanced protein levels of NOX4, α-sma, and α-collagen in lung tissue. The H_2O_2 content in lung tissue was also increased (Supplementary Fig. S3A, B).

Notably, these stimulatory effects of Ang(1–7) were markedly abolished by the AT1R blocker irbesartan (Supplementary Fig. S2A–D). In contrast, the presence of the selective Mas receptor inhibitor A779 greatly aggravated the stimulatory effects of Ang(1–7) (Supplementary Fig. S2A–D). In addition, combined treatment with irbesartan and A779 led to reduced levels of NOX4 protein and H_2O_2 production (Supplementary Fig. S2C, D), which were enhanced by Ang(1–7).

lentiACE2 reduced AngII-induced fibroblast migration and α-collagen I synthesis by inhibiting the NOX4/ROS/RhoA/Rock pathway

To determine whether the overexpression of ACE2 protected against the pro-migratory and pro-fibrotic effects induced by AngII in lung fibroblasts, the lung fibroblasts were infected with lentiACE2. As Figure 6 shows, lentiACE2 infection resulted in a twofold upregulation of ACE2 protein levels in lung fibroblasts (Fig. 6A). Furthermore, we found that lentiACE2 attenuated AngII-induced TGFβ mRNA and NOX4-dependent H_2O_2 and subsequently inhibited the activation of the RhoA/Rock pathway, resulting in the

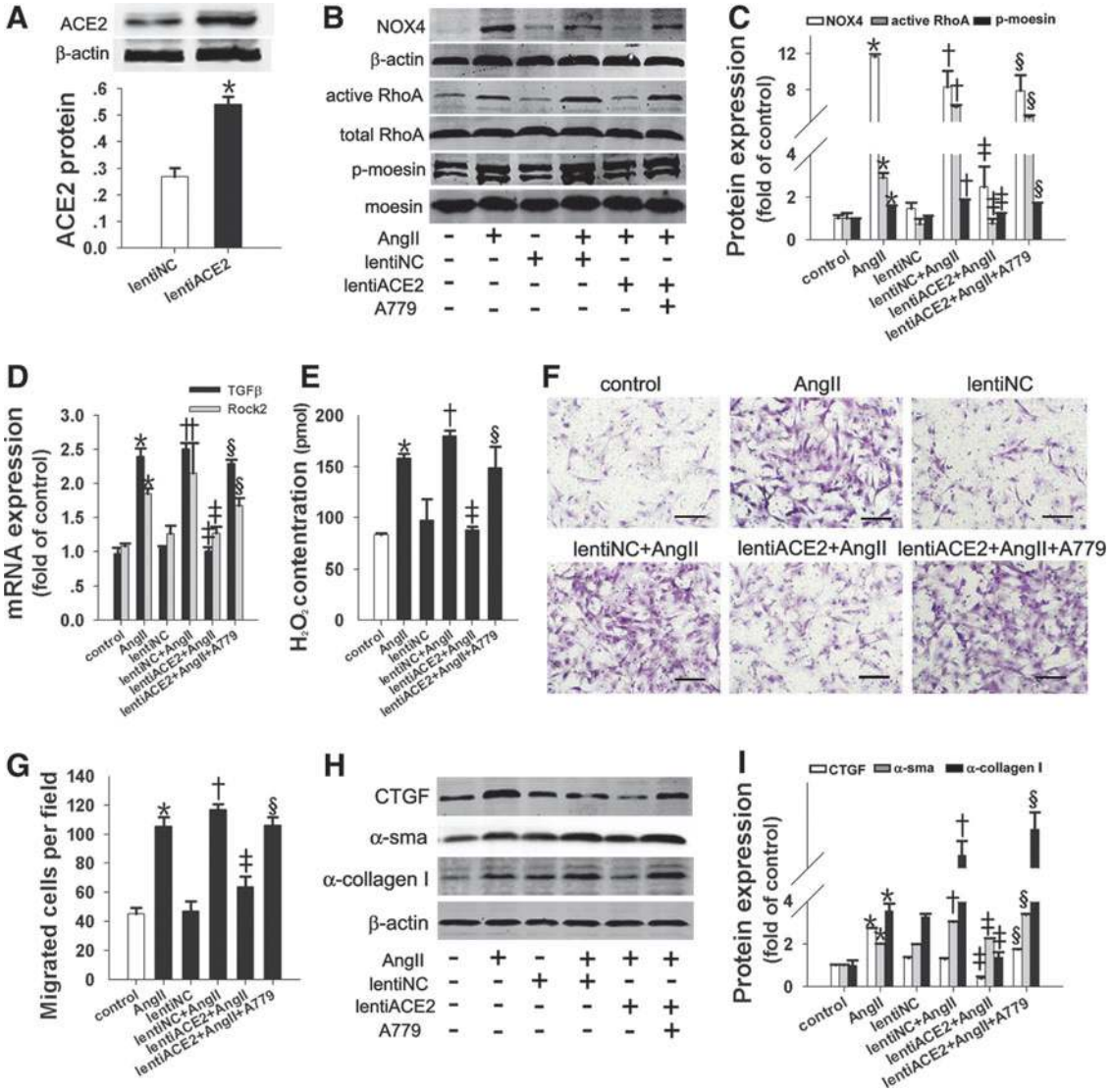

FIG. 6. Lenti-ACE2 suppressed AngII-induced fibroblast migration and α-collagen I synthesis by inhibiting the NOX4/ROS/RhoA/Rock pathway. Primary lung fibroblasts were infected with lenti-ACE2 for 96 h and then exposed to AngII (10^{-7} *M*) for 24 h after pretreatment with A779 for 1 h. **(A)** Overexpression of ACE2 was confirmed with Western blot. **(B, C)** Active RhoA was determined using the GST pull-down assay; NOX4 and p-moesin protein were detected with Western blot. **(D)** TGFβ and Rock2 mRNA levels were measured with real-time RT-PCR. **(E)** The H_2O_2 concentration was measured. **(F, G)** Lung fibroblast migration assays. **(H, I)** Western blot was performed to determine the CTGF, α-SMA, and α-collagen I protein levels. Data are the means ± SD of three independent experiments. Scale bar = 200 μm. $^{*}p < 0.05$ *versus* control; $^{\dagger}p < 0.05$ *versus* lentiNC; $^{\ddagger}p < 0.05$ *versus* AngII or lentiNC + AngII; $^{\S}p < 0.05$ *versus* lentiACE2 + AngII. ACE2, angiotensin-converting enzyme 2. To see this illustration in color, the reader is referred to the web version of this article at www.liebertpub.com/ars

suppression of lung fibroblast migration and α-collagen I synthesis (Fig. 6B–I). The inhibitory effects of lentiACE2 were partially blocked by A779, which revealed that ACE2 catalyzed the conversion of AngII into Ang(1–7), shedding light on the antimigratory and antifibrotic effects of ACE2 by inhibiting the NOX4/ROS/RhoA/Rock pathway.

BLM-induced pulmonary fibrosis in rats was attenuated by Ang(1–7) and exacerbated by AngII

To confirm our *in vitro* observation that the ACE/AngII/AT1R axis promoted collagen synthesis in lung fibroblasts while the ACE2/Ang(1–7)/Mas axis counteracted the pro-fibrotic effect, we established two animal models of BLM-induced lung fibrosis. In the first rat model, Ang(1–7) or AngII was continuously infused into BLM-treated rats using an osmotic minipump, and the lung tissues were analyzed at day 28. Compared with the control rats, BLM treatment alone was associated with higher Ashcroft scores and severe septal fibrosis, with a marked mononuclear infiltration and thickened alveolar septa throughout the lung parenchyma (Fig. 7A, C). Infusion with Ang(1–7) was associated with markedly lower scores and a reduced degree of fibrotic lesions (Fig. 7A, C). However, the pro-fibrotic effect was more evident in AngII-infused rats (Fig. 7A, C). In addition, lung collagen accumulation, as measured with Masson's trichrome, increased in BLM-treated rats. The

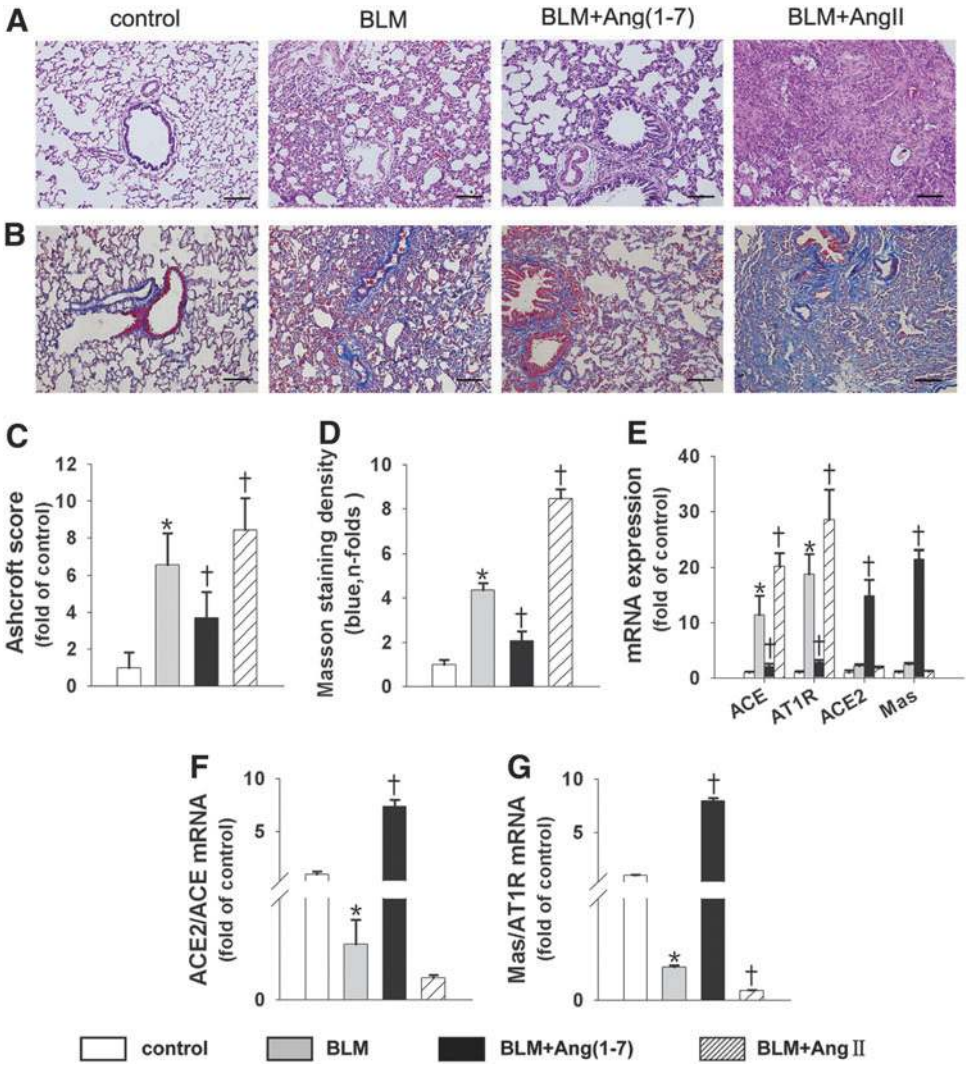

FIG. 7. BLM-induced pulmonary fibrosis was attenuated by Ang(1–7) and exacerbated by AngII, and the two axes of the RAS were affected differently. Representative microphotographs of lung sections from controls, BLM, BLM + Ang(1–7), and BLM + AngII ($n = 12$ rats per group) stained with H&E **(A)** and Masson's trichrome **(B)**. **(C)** Morphological changes in fibrotic lungs were quantified using the Ashcroft score. **(D)** Measurement of the collagen area in the Masson's trichrome-stained lungs of animals in the designated treatment groups. **(E)** The ACE, AT1R, ACE2, and Mas mRNA levels measured with real-time RT-PCR. **(F, G)** Bar graph representing the ACE2/ACE mRNA level ratio **(F)** and Mas/AT1 R mRNA level ratio **(G)**. Data are the mean ± SD. Scale bar = 200 μm. $^{*}p < 0.05$ *versus* controls, $^{\dagger}p < 0.05$ *versus* the BLM group. AT1R, angiotensinII type 1 receptor; BLM, bleomycin; RAS, renin-angiotensin system.

increase in collagen accumulation was significantly attenuated by Ang(1–7) infusion and was aggravated by AngII infusion (Fig. 7B, D).

The two axes of the RAS were differently affected by Ang(1–7) and AngII

The locally based RAS is involved in the development of lung fibrosis, and the ACE2/Ang(1–7)/Mas axis counteracts the pro-fibrotic effects of the ACE/AngII/AT1R axis (30). Hence, the balance of these two axes determines the development of pulmonary fibrosis. We then investigated the effects of Ang(1–7) or AngII on the two axes of RAS in BLM-treated rats. The results showed that BLM treatment resulted in increases of ~11.3-fold and 18.8-fold in the ACE and AT1R mRNA levels, respectively. However, BLM treatment augmented the ACE2 and Mas mRNA levels by ~2.2-fold and 2.4-fold, respectively, compared with the control group. Therefore, BLM treatment shifted the balance toward the ACE/AngII/AT1R axis. Moreover, AngII treatment promoted the ACE and AT1R levels by ~1.8-fold and 1.5-fold, respectively, compared with the BLM group; however, the expression of ACE2 and Mas slightly decreased (Fig. 7E). Interestingly, Ang(1–7) increased the ACE2 and Mas levels by ~6.8-fold and 8.9-fold, respectively, while it significantly decreased the ACE and AT1R levels compared with the BLM group (Fig. 7E). Therefore, Ang(1–7) treatment resulted in an ~33.7-fold increase in the ACE2/ACE ratio and an ~61.5-fold increase in the Mas/AT1R ratio (Fig. 7F, G). Overall, Ang(1–7) treatment shifted the balance from the ACE/AngII/AT1R axis toward the ACE2/Ang/(1–7)/Mas axis in fibrotic rat lungs.

The NOX4/ROS/RhoA/Rock pathway in BLM-induced lung fibrosis in rats was differently affected by Ang(1–7) and AngII

We examined whether Ang(1–7) attenuated BLM-induced lung fibrosis by inhibiting the NOX4/ROS/RhoA/Rock pathway. The NOX4 protein level and H_2O_2 content in the lungs were markedly enhanced in the BLM group compared with the control group (Fig. 8B, D), whereas other NOX isoform protein levels showed no differences between the BLM group and the control group (Fig. 8A). The BLM-induced NOX4 protein and H_2O_2 production levels were markedly reduced by Ang(1–7) treatment and augmented by AngII treatment (Fig. 8B, D, F). Moreover, NOX4 co-localized with α-sma in the myofibroblastic foci of lung

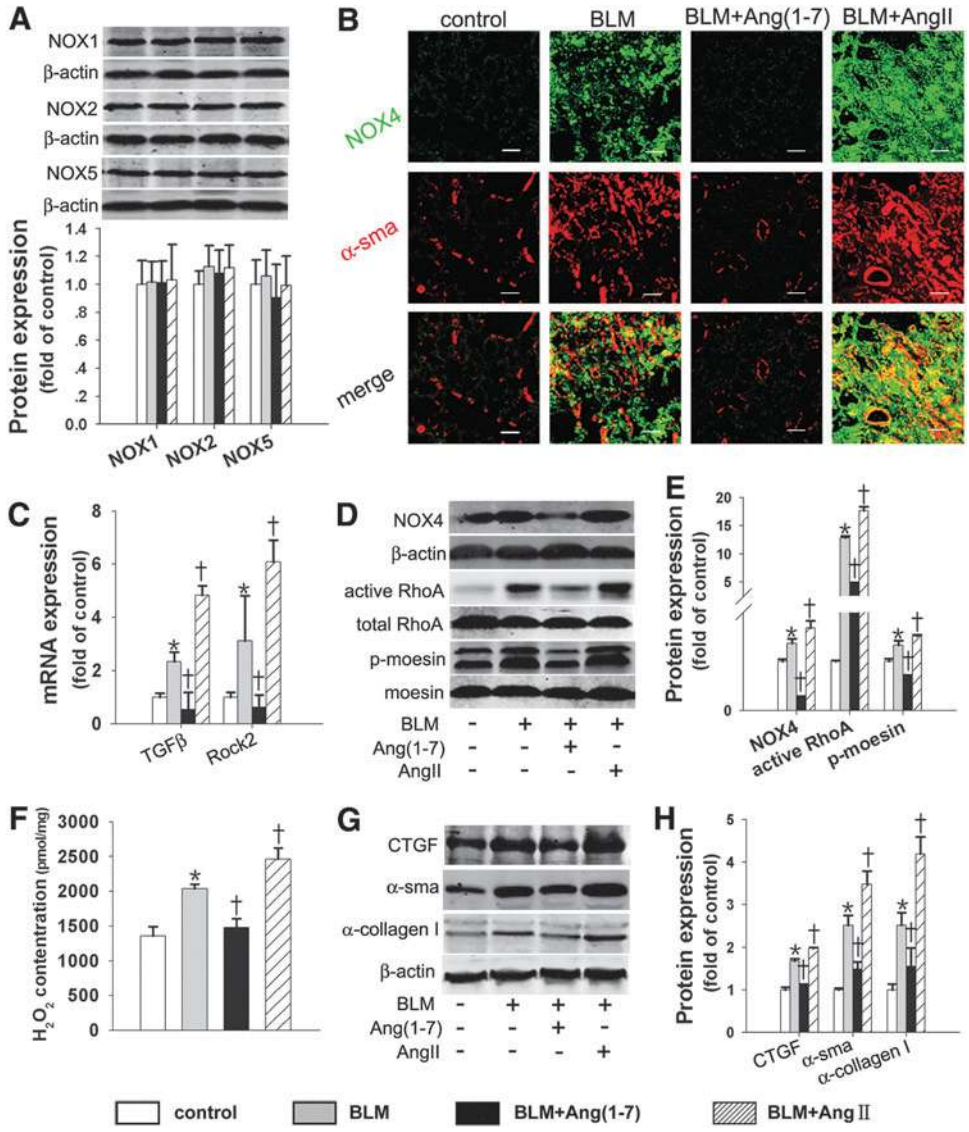

FIG. 8. The NOX4/ROS/RhoA/Rock pathway and α-collagen I synthesis in BLM-induced lung fibrosis were affected differently by Ang(1–7) and AngII. (A) Western blot was performed to measure the NOX1, NOX2, and NOX5 protein levels. **(B)** Dual immunofluorescence of NOX4 (*green*) and α-sma (*red*). **(C)** The TGFβ and Rock2 mRNA levels were measured with real-time RT-PCR. **(D, E)** Active RhoA was determined using the GST pull-down assay; NOX4 and p-moesin proteins were detected with Western blot. **(F)** The H_2O_2 concentration in the lung tissue was measured. **(G, H)** Western blot was performed to measure the CTGF, α-SMA, and α-collagen I protein levels. Data are the means ± SD. Scale bar = 200 μm. $^{*}p < 0.05$ *versus* control group; $^{\dagger}p < 0.05$ *versus* BLM.

fibrotic tissue (Fig. 8B), supporting the idea that NOX4 mediated the fibrotic effects of lung fibroblasts. In keeping with the *in vitro* findings, the signaling molecules (active RhoA protein, Rock2 mRNA, and p-moesin protein) were markedly reduced by Ang(1–7) treatment and were augmented by AngII treatment (Fig. 8C–E). Similarly, Ang(1–7) reduced the CTGF, α-sma, and α-collagen I protein levels induced by BLM, which were aggravated by AngII treatment (Fig. 8G, H). Hence, Ang(1–7) attenuated BLM-induced lung fibrosis by inhibiting the NOX4/ROS/RhoA/Rock pathway.

ACE2 overexpression attenuated BLM-induced pulmonary fibrosis and shifted the RAS toward the ACE2/Ang(1–7)/Mas axis

In the second rat model, lentiNC or lentiACE2 was preinstilled into the trachea in BLM-treated rats. The lentiNC + BLM group showed severe fibrotic lesions, including the loss of lung architecture and lung fibrosis in the parenchyma at a level similar to that caused by BLM treatment alone. However, lentiACE2 treatment was associated with significantly lower Ashcroft scores (Fig. 9A, C) and markedly decreased deposition of collagen (Fig. 9B, D, E). Our data also indicate the effects of lentiACE2 on the RAS components. As Figure 9F–J shows, lentiACE2 treatment resulted in the prevention of increases in ACE protein, ACE, and AT1R mRNA compared with the BLM and lentiNC groups (Fig. 9F–H). However, ACE2 protein, ACE2, and Mas mRNA levels were significantly higher in the lentiACE2 treatment group (Fig. 9F–H).Therefore, lentiACE2 treatment resulted in an increase of ~17-fold in the ACE2/ACE ratio and ~6-fold in the Mas/AT1 receptor ratio compared with the BLM and lentiNC groups (Fig. 9I, J). Collectively, these data suggest that ACE2 overexpression facilitates shifting the balance of RAS from the pro-fibrotic ACE/AngII/AT1R axis toward the antifibrotic ACE2/Ang(1–7)/Mas axis.

ACE2 overexpression protected against BLM-induced lung fibrosis by inhibiting the NOX4/ROS/RhoA/Rock pathway

Finally, we found that other NOX isoform protein levels in lung tissue were not affected by lentiACE2 (Fig. 10A). The increases in NOX4 protein and H_2O_2 production were

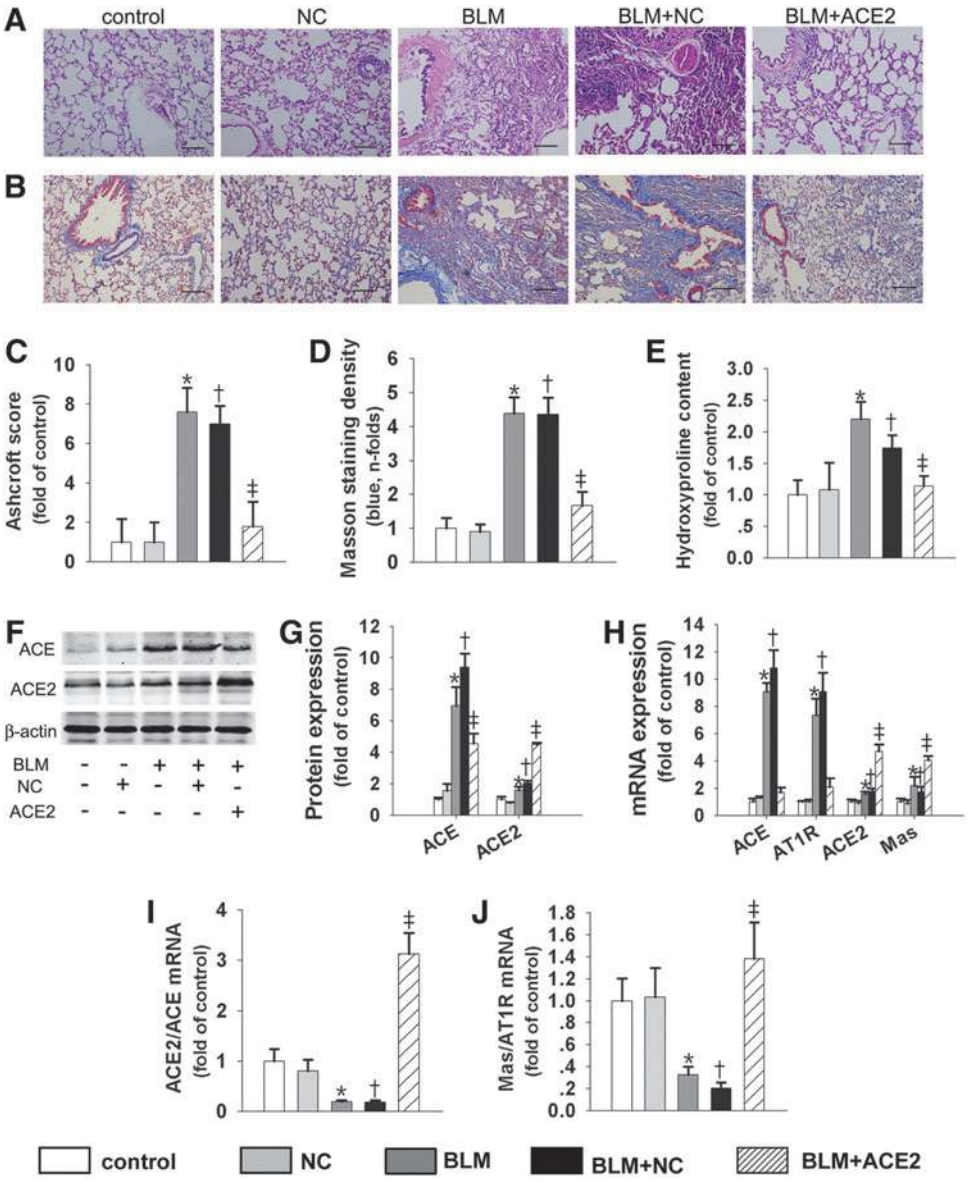

FIG. 9. ACE2 overexpression attenuated BLM-induced pulmonary fibrosis and shifted the RAS toward the ACE2/Ang(1–7)/Mas axis. Representative microphotographs of lung sections from controls, BLM, BLM + lentiNC, and BLM + lentiACE2 ($n = 12$ rats per group) stained with H&E **(A)** and Masson's trichrome **(B)**. **(C)** Morphological changes in fibrotic lungs were quantified using the Ashcroft score. **(D)** Measurement of the collagen area in the Masson's trichrome-stained lungs of animals in the designated treatment groups. **(E)** Hydroxyproline content in the various treatment groups. **(F, G)** ACE and ACE2 protein expression was detected using Western blot. **(H)** The ACE, AT1R, ACE2, and Mas mRNA levels were measured using real-time PCR. The bar graph represents ACE2/ACE **(I)** and Mas/AT1 R mRNA levels **(J)**. Data are the means ± SD. Scale bar = 200 μm. $^{*}p < 0.05$ *versus* control group, $^{\dagger}p < 0.05$ *versus* NC group, $^{\ddagger}p < 0.05$ *versus* BLM + NC group.

significantly reduced by lentiACE2 treatment (Fig. 10B, D, E, F). Moreover, lentiACE2 treatment showed less co-localization of NOX4 and α-sma in lung tissue (Fig. 10B). Similarly, the signaling molecules were markedly inhibited by lentiACE2 treatment (Fig. 10D–F). We also found that lentiACE2 reduced the increases in CTGF, α-sma, and α-collagen I protein levels induced by BLM (Fig. 10G, H). Overall, these results suggest that ACE2 overexpression attenuates BLM-induced lung fibrosis by inhibiting the NOX4/ROS/RhoA/Rock pathway.

Discussion

This study provides four novel conclusions regarding the role of oxidase stress in the pro-fibrotic effects of the ACE/AngII/AT1R axis and the anti-fibrotic effects of the ACE2/Ang(1–7)/Mas axis. First, NOX4-dependent ROS caused by the activation of the ACE/AngII/AT1R axis contributes to the development of AngII- or BLM-induced lung fibrosis. Second, NOX4-dependent ROS are required for AngII-induced lung fibroblast migration and α-collagen I synthesis, because they activate the RhoA/Rock pathway. Third, Ang(1–7) and lentiACE2 treatment protect against BLM-induced pulmonary fibrosis by shifting the balance of the RAS toward the ACE2/Ang(1–7)/Mas axis and by inhibiting the generation of ROS. Fourth, Ang(1–7) and lentiACE2 protect against BLM- or AngII-induced lung fibroblast migration and ECM accumulation by inhibiting the NOX4-derived ROS-mediated RhoA/Rock pathway.

The ROS play important roles in the pathogenesis of IPF and BLM-induced lung fibrosis (15, 20). Consistent with these findings, we found that BLM treatment increased ROS production *in vivo*, and the ROS scavenger NAC decreased collagen secretion *in vitro*, which is similar to the report that NAC protects against BLM-induced lung fibrosis (15). However, the mechanisms underlying elevated ROS in BLM-induced lung fibrosis remain unclear. The ACE/AngII/AT1R axis was shown to increase oxidative stress in kidney (57), cardiac (58, 59), and hepatic fibrosis (5). We propose that the pro-oxidant effect of BLM may be associated with the

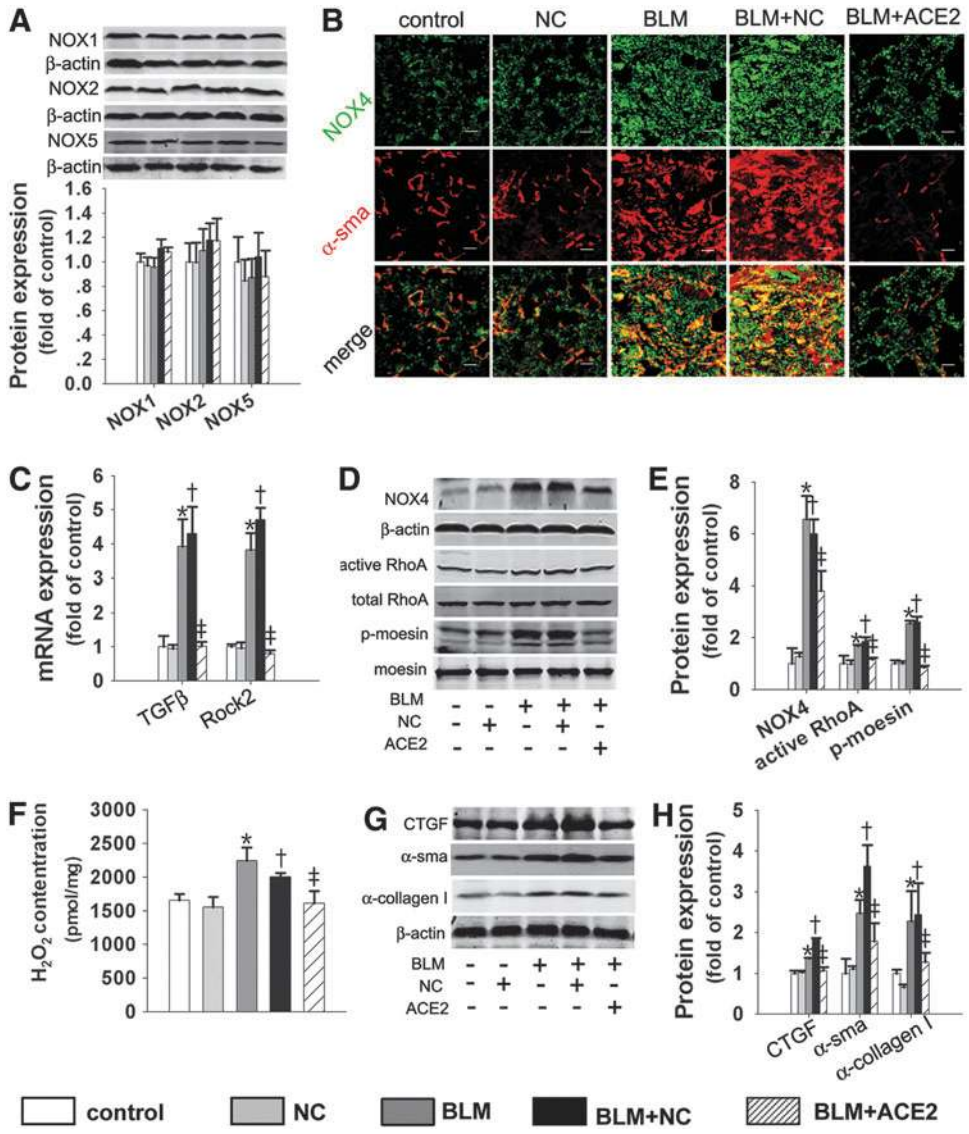

FIG. 10. ACE2 overexpression protected against BLM-induced lung fibrosis by inhibiting the NOX4/ROS/RhoA/Rock pathway. **(A)** The NOX family protein levels were measured with Western blot. **(B)** Dual immunofluorescence of NOX4 (*green*) and α-sma (*red*). **(C)** The TGFβ and Rock2 mRNA levels were measured using real-time RT-PCR. **(D, E)** Active RhoA was determined using the GST pull-down assay; NOX4 and p-moesin proteins were detected with Western blot. **(F)**The concentration of H_2O_2 was measured. **(G, H)** Western blot was performed to measure the CTGF, α-SMA, and α-collagen I protein levels. Data are the means ± SD. Scale bar = 200 μm. $^{*}p < 0.05$ *versus* control group; $^{\dagger}p < 0.05$ *versus* NC group. $^{\ddagger}p < 0.05$ *versus* BLM + NC group.

augmentation of ACE and AT1R levels. The ACE/AngII/AT1R axis is upregulated during the lung fibrosis process, and the AT1R inhibitor protects against lung fibrosis (25, 28). In support of these findings, we found that ACE and AT1R mRNA levels were significantly increased in the lungs of BLM-treated rats, indicating a hyperactive RAS, especially the ACE/AngII/AT1R axis in the lung. Moreover, constant infusion with exogenous AngII significantly aggravated BLM-induced lung fibrosis and markedly promoted the generation of ROS, which is consistent with previous studies showing that AngII promoted ROS production in kidney (57) and hepatic fibrosis (5). In contrast, we found that the AT1R inhibitor irbesartan decreased ROS production, and the ROS scavenger NAC attenuated α-collagen I synthesis induced by AngII in lung fibroblasts. Hence, these findings suggest that ROS generation arising from the activation of the ACE/AngII/AT1R axis contributes to the development of AngII- or BLM-induced lung fibrosis.

Although ROS generation is required for AngII- or BLM-induced lung fibrosis, the precise cellular source of ROS generation remains incompletely elucidated. In cells, the ROS are generated from several enzymatic sources, but the most significant producers of oxidants are NOXs and mitochondria. Recent studies have shown that NADPH-dependent ROS generation is required for TGFβ-induced pro-fibrotic responses in lung fibroblasts, and much interest has been focused on these enzymes in the lungs (1, 17). NOX enzymes catalyze the reduction of molecular oxygen to superoxide, but the activities of different NOX isoforms are subject to very different modes of regulation. NOX1 and NOX2 are acutely regulated by post-translational mechanisms, such as the phosphorylation of regulatory subunits induced by agonist activities (8, 24). However, NOX4 activity is constitutive and dependent on its levels of gene transcription and protein expression (8, 29), and ROS generation is inducible at the gene transcription level rather than at the level of acute post-translational mechanisms (39). NOX4 gene transcription and protein expression were reported to be upregulated in response to AngII (49, 52). Consistent with these findings, we found that the NOX4 mRNA or protein levels induced by BLM or AngII were markedly upregulated among the four isoforms of NOX. In

contrast, the NOX1, NOX2, and NOX5 mRNA or protein levels induced by AngII or BLM did not significantly increase compared with those of the control group, suggesting those levels are most likely regulated by a post-translational mechanism.

As a cytosolic subunit of NOX isoforms, the role of Rac1 in AngII-induced NOX4 activation in lung fibroblasts remains unknown. Current evidence suggests that NOX4 heterodimerization with p22phox is sufficient to enhance the enzyme activity, and it does not require cytosolic subunits that are essential for other NOX isoforms (2). However, this study showed that AngII treatment increased active Rac1 protein levels in lung fibroblasts and enhanced the interactions between NOX4 and Rac1. Furthermore, the Rac1 inhibitor Ehop significantly reduced AngII-induced protein levels of NOX4 and α-collagen I. These data are consistent with Wu RF's report that Rac1 regulated NOX4 function in endothelial cell (50). Hence, Rac1 plays a potential role in AngII-induced NOX4 activation and consequent α-collagen I synthesis; further studies are needed.

In addition, in lung fibroblasts stimulated with AngII, both pharmacological treatment with specific inhibitors (DPI) and genetic interference from NOX4 substantially decreased the production of ROS and fibrogenesis markers, such as α-sma and α-collagen I. These data suggest that the change in NOX4-derived ROS production depends on the levels of NOX4 gene transcription and protein expression and contributes to AngII-induced pulmonary fibrosis. However, others have reported that some NOX4 knockout mice experienced enhanced oxidative stress, resulting in exaggerated kidney fibrosis (35), which may be explained by the multiple roles that NOX4 plays in different tissue types. Notably, since other NOX isoforms (such as NOX2) are a key source of ROS production, the contribution from NOX2-driven signaling cannot be completely ruled out in AngII-induced pulmonary fibrosis. Therefore, further studies are needed to identify the effects of NOX2 on pulmonary fibrosis induced by AngII and the effects of NOX4 on fibrosis in different tissues.

The migration of lung fibroblasts is the initial step of lung fibrosis (43), and oxidative stress is required for this process (3). The lung fibroblasts migrate to inflammatory sites, accumulate in the injured area, and secrete ECM, leading to lung fibrosis. Increased ROS production is known to promote cell migration through the regulation of cytoskeleton reorganization (18). Nevertheless, the role of NOX4-derived ROS in lung fibroblast migration induced by AngII has not been previously reported. Our study showed that DPI, NOX4 siRNA, and NAC abrogated AngII-stimulated lung fibroblast migration, indicating that NOX4-derived ROS are directly correlated with AngII-induced lung fibroblast migration.

Small Rho GTPases, such as RhoA, play key roles in α-collagen I synthesis (21, 33) and cell migration (9, 46) by modulating actin polymerization, which contributes to lung fibrosis. However, little is known about the role of the RhoA/Rock pathway in AngII-induced lung fibrosis. We found that active RhoA protein, Rock2 mRNA, and p-moesin protein were activated by BLM or AngII both *in vivo* and *in vitro*. Furthermore, AngII-induced lung fibroblast migration and α-collagen I synthesis may be inhibited by the Rock inhibitor Y27632. Hence, AngII stimulates lung fibroblast migration and collagen secretion *via* the RhoA/Rock pathway. Evidence in the literature suggests that RhoA is a downstream intermediate of ROS-dependent AngII-induced VSMC migration (31) and hyperoxia-induced collagen synthesis (21). Consistent with these reports, we found that DPI, NOX4 siRNA, and NAC treatment inhibited AngII-induced RhoA activation in lung fibroblasts, indicating that the AngII-induced RhoA/Rock pathway is mediated by NOX4-dependent ROS. In contrast, others have shown that NOX1-derived ROS downregulated RhoA activity in RAS-transformed normal rat kidney cells (42). Therefore, the effect of ROS on RhoA activation appears to be cell specific.

In this study, we similarly showed that BLM-induced collagen deposition in the lungs was significantly attenuated by Ang(1–7) or lentiACE2 treatment. Nevertheless, the exact molecular mechanism by which the ACE2/Ang(1–7)/Mas axis counteracts the pro-fibrotic effects and whether ROS production is inhibited by Ang(1–7) or ACE2 in the lungs remain unclear. As demonstrated earlier, the upregulation of the ACE/AngII/AT1R axis has been revealed to increase the ROS levels in the lung. Notably, we found that Ang(1–7) and ACE2 directly reduced the ACE and AT1R mRNA levels in the lungs of BLM-treated rats, resulting in the shift of the RAS pathway toward the ACE2/Ang(1–7)/Mas axis. Next, we asked whether the counteracting effect of the ACE2/Ang(1–7)/Mas axis has an antioxidant effect. For the first time, this study demonstrated that the elevated levels of NOX4 protein and ROS production were decreased by Ang(1–7) or lentiACE2 in BLM-treated rats or AngII-stimulated lung fibroblasts. These results support the recent findings that the ACE2/Ang(1–7)/Mas axis inhibits AngII-mediated ROS generation and transcriptional activity in the kidney (31), brain (51), and cardiovascular system (59). Moon JY reported that Ang(1–7) treatment attenuated AngII-mediated NOX activation and ROS production in diabetic glomeruli and mesangial cells (32). In addition, rhACE2 inhibited AngII-mediated myocardial fibrosis by reducing AngII-induced superoxide production (59). ACE2 overexpression resulted in the reduction of AngII-induced NOX in the paraventricular nucleus of ACE2-deletion mice, and ACE2 knockout promoted age-dependent oxidative stress in the brain (51). Hence, the upregulation of the ACE2/Ang(1–7)/Mas axis inhibited lung fibrosis by reducing NOX4-dependent ROS production.

As demonstrated earlier, the NOX4/ROS/RhoA/Rock pathway plays an essential role in AngII- or BLM-induced lung fibroblast migration and ECM accumulation. We proposed that Ang(1–7) and ACE2 protect against pulmonary fibrosis by inhibiting the NOX4/ROS/RhoA/Rock pathway. As expected, the results presented in this article support that Ang(1–7) attenuated BLM- or AngII-induced lung fibroblast migration and collagen secretion by inhibiting the NOX4-derived ROS-mediated RhoA/Rock pathway. In addition, the inhibitory effects of Ang(1–7) may be blocked by A779, the Mas inhibitor, suggesting that Ang(1–7) counteracted AngII *via* the Mas receptor. Similarly, we observed that the overexpression of ACE2 alleviated the pro-migratory and pro-fibrotic effects of AngII. ACE2 cleaves its substrate, AngII, into the heptapeptide Ang(1–7), and ACE2 exerts its protective effects by simultaneously reducing the detrimental effects of AngII and increasing the beneficial effects of Ang(1–7). This finding is supported by our observation that the suppressive effects of ACE2 are reversed by A779. Overall, these data provide evidence which suggests that the ACE2/Ang(1–7)/Mas axis attenuates BLM- or AngII-induced lung fibroblast

migration and collagen deposition by inhibiting the NOX4/ROS/RhoA/Rock pathway.

Interestingly, we observed that Ang(1–7) alone increased lung fibroblast migration and α-collagen I synthesis by activating the oxidative stress-dependent RhoA pathway. The reasons for the contradictory effects of Ang(1–7) are currently unclear. To an extent, the variable responses to Ang(1–7) depend on the state of local RAS activation. When the ACE/AngII/AT1R axis is activated by BLM or AngII, exogenous Ang(1–7) significantly downregulates the ACE/AngII/AT1R axis, which may cause a significant reduction in AngII levels and lead to the attenuation of lung fibrosis. In addition, exogenous Ang(1–7) upregulates the ACE2/Ang(1–7)/Mas axis, thereby facilitating the hetero-oligomerization of Mas (a physiological antagonist of AT1R) with AT1R and thus interfering with AngII action (23), and the inhibitory effects of Ang(1–7) could be abolished by A779 in lung fibroblasts. Hence, Ang(1–7) exerts its beneficial effect *via* the Mas receptor.

In contrast, we found that Ang(1–7) alone initiated oxidative stress both *in vivo* and *in vitro* and thus resulted in fibroblast migration and α-collagen I synthesis in the event of the failure of the ACE/AngII/AT1R axis activation by BLM or AngII treatment. We hypothesized that Ang(1–7) may cross-talk with AT1R in addition to combining with the Mas receptor. To verify this hypothesis, we observed the effects of the AT1R inhibitor losartan or the Mas antagonist A779 on Ang(1–7)-induced pro-oxidant and pro-fibrotic effects in lung fibroblasts. We found that pretreatment with A779 aggravated the pro-oxidant and pro-fibrotic effects of Ang(1–7). In contrast, pretreatment with losartan markedly abolished the detrimental effects of Ang(1–7), which is consistent with Giani's study that showed that Ang(1–7)-induced STAT3 and 5a/b phosphorylation could be blocked with losartan (13). Hence, Ang(1–7) may cross-talk with AT1R and exert its detrimental effects; meanwhile, Ang(1–7) exerts its beneficial effects by combining with its Mas receptor. Considering the ultimate effects of Ang(1–7) alone in lung fibroblasts, AT1R seems to have a greater advantage over the Mas receptor in lung fibroblasts.

Nevertheless, the divergent effects of Ang(1–7) alone have been reported. Ni found that Ang(1–7) alone inhibited the migration of A549 cells by inactivating the PI3K/Akt and the MAPK signaling pathways (34), and it reduced fibrosis in the tumor microenvironment by reducing MAPK activity (12). The different effects of Ang(1–7) might be explained by differences between cell types. The exact molecular mechanism of Ang(1–7)/Mas signaling in different cell types requires further elucidation.

There are some limitations to this study. Although this study could potentially be relevant to clinical therapy for pulmonary fibrosis, the effects of the ACE2/Ang(1–7)/Mas axis on pulmonary fibrosis were not evaluated in patients with that condition. Future studies will focus on the role of the ACE2/Ang(1–7)/Mas axis in treatments for pulmonary fibrosis patients.

In summary, our study first demonstrated NOX4-derived ROS-mediated BLM-, or AngII-induced lung fibroblast migration and lung fibrosis *via* the RhoA/Rock pathway. Constant infusion of Ang(1–7) and lentivirus-mediated ACE2 overexpression protected against BLM- or AngII-induced pulmonary fibrosis by downregulating the NOX4/ROS/RhoA/Rock pathway (Supplementary Fig. S4). This study suggests that the ACE2/Ang(1–7)/Mas axis could be a novel pharmacological antioxidant target for lung fibrosis induced by AngII-mediated ROS.

Materials and Methods

Materials

AngII, Ang(1–7), A779 (a selective Mas receptor inhibitor), DPI (an NADPH-oxidase inhibitor), NAC (a superoxide inhibitor), irbesartan (an AT1R blocker), and Ehop (an Rac1 inhibitor) were purchased from Sigma-Aldrich. The reactive oxygen species assay kit (DCF-DA) was purchased from Applygen. The hydrogen peroxide assay kit was purchased from Biovision. Active Rho Pull-Down and Detection Kits were purchased from Thermo Scientific. The Rac1/Cdc42 Activation Assay Kit was purchased from Biovision. BLM was purchased from Nippon Kayaku. Alzet osmotic pumps (models 2004 and 2ML4) were purchased from the Durect Corporation. Lenti Empty and ACE2 virus were provided by Genechem. NOX4-siRNA was provided by GenePharma.

Animals

All experimental procedures using rats were approved by the Committee on the Ethics of Animal Experiments of Southern Medical University and were performed in accordance with the World Medical Association's Declaration of Helsinki. Male Wistar rats (200–300 g) were purchased from the Central Animal Care Facility of Southern Medical University (Permission No. SCXK 2009-015). The animals were housed (12 h light/dark; temperature, 22°C–24°C) and given food and water *ad libitum*.

Treatment regimens

We established three animal models. The first model was performed as previously described (30). In the first model, 48 male Wistar rats were randomly divided into four groups of 12 rats each: a control group, a BLM treatment group, a BLM + Ang(1–7) treatment group, and a BLM + AngII treatment group. All of the rats received a single intratracheal instillation of 200 μl of sterile saline while under pentobarbital anesthesia. The three BLM groups received sterile saline that contained 5 mg/kg of BLM sulfate. While the animals were under anesthesia, micro-osmotic pumps were subcutaneously implanted to permit 28 days of continuous infusion with AngII or Ang(1–7) at a rate of 25 $\mu g/kg^{-1} \cdot h^{-1}$. The animals in the control and BLM treatment groups received constant subcutaneous saline infusions.

In the second model, sixty male Wistar rats received 3×10^8 TU lenti-empty virus (lentiNC) or lenti-CE2 *via* intratracheal instillation under pentobarbital anesthesia. Two weeks after lentiviral treatment, the animals were subjected to BLM (5 mg/kg in 300 μl of sterile saline). The control animals received an equal volume of sterile saline or lentiNC.

In the third model, 28 male Wistar rats were also treated as previously described (30).

Histological assessment

The right lung was fixed using an intratracheal instillation of 4% paraformaldehyde and embedded in paraffin. Sections

were stained with hematoxylin and eosin or with Masson's trichrome and examined with light microscopy. Histopathological scoring of pulmonary fibrosis was performed according to the method reported by Ashcroft *et al.* (4), and the presence of collagen was assessed by analyzing the stained area as a percentage of the total area.

Immunofluorescent histochemistry

Tissue samples were sectioned, deparaffinized, and processed for staining. The tissue was incubated with anti-Nox4 antibody (1:100) and anti-α-sma antibody (1:300). After probing with the appropriate fluorescein isothiocyanate-conjugated and Cyt3-conjugated antibodies, the fluorescent signals were detected using an Olympus FV10i-W confocal microscope.

Hydroxyproline assay

The concentration of hydroxyproline was measured according to the manufacturer's instructions (Hydroxyproline Assay Kit; Sigma).

Isolation of primary lung fibroblast

Normal rat primary fibroblasts were generated by culturing the lungs of male Wistar rats as previously described (48). The cells were cultured in Dulbecco's modified Eagle's medium (DMEM) supplemented with 15% fetal bovine serum (Gibco). After 6 h of serum starvation, the fibroblasts were pretreated for 1 h with irbesartan (10^{-5} *M*), A779 (10^{-5} *M*), DPI (10^{-5} *M*), or NAC (10^{-3} *M*) before exposure to AngII (10^{-7} *M*) for the indicated times. The cells infected with lentiNC or lentiACE2 were treated with AngII (10^{-7} *M*) or A779 (10^{-5} *M*). The cells that were used to detect the p-moesin protein level were stimulated for 30 min.

Migration assay

Cell migration assays were performed using Corning cell culture inserts as previously described (31). Microphotographs of nine different fields were taken, and the cells were counted. The average number of migrating cells was determined for each experimental condition.

Intracellular ROS detection

Intracellular ROS production was quantified using the oxidation-sensitive probe 2,7-dichlorofluorescein diacetate (DCF-DA) (Applygen). Briefly, 10 m*M* DCF-DA stock solution (in methanol) was diluted 1000-fold in cell culture medium without serum to yield a 10-μm working solution. After 24 h of stimulation, the cells in 24-well plates were washed twice with phosphate-buffered saline (PBS) and incubated in 500 μl working solution of DCF-DA at 37°C in dark for 1 h. The cells were then washed twice with cold PBS and resuspended in the PBS for an analysis of intracellular ROS using a multiwell fluorescence scanner (SpectraMax M5/M5e; Molecular Devices) and microscope (Olympus). DCF-DA fluorescence was detected at an excitation wavelength of 480 nm and an emission wavelength of 525 nm (5).

H_2O_2 assay

The H_2O_2 concentration was assessed using a Hydrogen Peroxide Assay Kit (Biovision; K265-200). The cells were dispersed and centrifuged to obtain a cell pellet; the supernatant was discarded, and the cell pellet was kept at −80°C for several hours. Next, the cell pellet was resuspended in 100 μl of lysis buffer containing protease inhibitor and centrifuged at 12,000 *g* for 3 min at 4°C. The right lung lobes (10 mg) were ground with liquid nitrogen, homogenized in 100 μl of lysis buffer containing protease inhibitor, and centrifuged at 12,000 *g* for 3 min at 4°C. Then, 50 μl of the reaction mix (48 μl Assay Buffer, 1 μl OxiRed™ Probe solution and 1 μl HRP solution) was added to each well, followed by 50 μl of supernatant. The wells were mixed gently and incubated at room temperature for 10 min. Finally, fluorescence was detected using a multiwell fluorescence scanner (SpectraMax M5/M5e; Molecular Devices) at an excitation wavelength of 535 nm and an emission wavelength of 587 nm. The concentration of released H_2O_2 was calculated based on the standard concentration curve of triplicate experiments.

RhoA pull-down assay

The cells were lysed on the culture plate with 0.5 ml lysis/binding/wash buffer with inhibitors. Next, the cells were scraped off the plate. The suspensions were centrifuged for 15 min at 16,000 *g* at 4°C. The clarified cell lysates (500 μg) were incubated with 400 μg GST-Rhotekin-RBD bound to glutathionine coupled-agarose beads at 4°C for 1 h and then centrifuged at 6000 *g* for 30 s. After being washed thrice with 400 μl lysis/binding/wash buffer, the rensin was added to 50 μl of 2× SDS sample buffer that contained 2.5 μl of β-mercaptoethanol. Half of each elution was analyzed using SDS-PAGE and detected with Western blotting using the specific RhoA-GTPase primary antibody.

Rac1 pull-down assay

Active Rac1 protein was measured with reference to the RhoA pull-down assay.

Cell transfection with siRNA

To suppress endogenous NOX4 expression, the experiments utilized a specific siRNA (sense 5-GGACCUUUGU GCCUAUACUTT-3; antisense 5-AGUAUAGGC ACAAA GGUCCTT-3) against NOX4 designed against the target region of the NOX4 gene. Scrambled siRNA (nonhomologous to the rat genome) was used as the control. The cells were transfected as previously described (37).

Production of lentiACE2 viral particles

Lentiviral particles containing enhanced green fluorescent protein (pGC-FU-GFP, lenti-GFP/lenti-NC) or rat ACE2 (pGC-FU-ACE2-GFP, lenti-ACE2) were prepared as described in our previous study (30). Viral medium containing lentiGFP or lentiACE2 was collected, concentrated, and titered. The concentration of viral particles was determined with Western blotting. The efficacy of lentiACE2 in producing active ACE2 enzymes has been previously established.

Immunofluorescent cytochemistry

Primary rat lung fibroblast on glass coverslips was processed as previously described (47). The cells were incubated

with anti-Nox4 antibody (1:100) and anti α-sma antibody (1:300) for 14 h at 4°C and then incubated with fluorescein isothiocyanate-conjugated and Cyt3-conjugated secondary antibodies for 1 h at 37°C. Fluorescence was visualized using an OLYMPUS FV10i-W confocal microscope. Controls with no primary antibody showed no fluorescence labeling, and single label controls were performed in the double-labeling experiments.

Immunoprecipitation analysis of Rac1 and NOX4

Homogenates from AngII-stimulated lung fibroblast were adjusted to an equal protein concentration (1 mg/ml), precleared, and then incubated with 2 μg/ml of anti-Rac1 antibody overnight at 4°C. Rac1 and NOX4 immune complexes were immunoprecipitated with protein agarose beads for 2 additional hours. Immunoprecipitates were resolved in SDS–polyacrylamide gels. Immunoblottings of NOX4 immunoprecipitates were undertaken with anti-Rac1 antibody.

Western blot analysis

Western blot was performed as previously described (30) with use of the following antibodies: α-collagen I, α-sma, CTGF (1:1000; Abcam); NOX1, NOX2, NOX5 (1:1000; Biovision), NOX4, RhoA (1:1000; Abcam); p-moesin, moesin (1:1000; Cell Signaling Technology); and β-actin (1:1000; ZSGB-Bio Origene), Rac1, and cdc42 (Millipore). All Western blots were repeated at least thrice.

Quantitative real-time polymerase chain reaction analysis

TGFβ and Rock2 mRNA was quantified with quantitative real-time RT-PCR as previously described (30). PCRs consisting of 95°C for 10 min (1 cycle), 95°C for 15 s, and 60°C for 1 min, 72°C for 30 s (40 cycles) were performed on an ABI Prism 7500 Sequence Detection System (Applied Biosystems). mRNA expression was normalized to that of GAPDH.

Statistical analysis

All data are presented as the means ± standard deviation. Significant differences were evaluated by ANOVA followed by multiple-comparison testing (with the Student–Neuman–Keuls and least-significant difference tests). *p*-Values less than 0.05 were considered statistically significant. All of the data were analyzed using SPSS 13.0®.

Acknowledgment

This study was supported by research grants from the National Science Foundation of China (30900659, 81370158). We thank Prof. Ping-Sheng Wu and Prof. Ji-Man He for their kind help to this study.

Author Disclosure Statement

The authors do not have any commercial associations that might create a conflict of interest in connection with this article.

References

1. Amara N, Goven D, Prost F, Muloway R, Crestani B, and Boczkowski J. NOX4/NADPH oxidase expression is increased in pulmonary fibroblasts from patients with idiopathic pulmonary fibrosis and mediates TGFbeta1-induced fibroblast differentiation into myofibroblast. *Thorax* 65: 733–738, 2010.
2. Ambasta RK, Kumar P, Griendling KK, *et al.* Direct interaction of the novel Nox proteins with p22phox is required for the formation of a functionally active NADPH oxidase. *J Biol Chem* 279: 45935–45941, 2004.
3. Artaud-Macari E, Goven D, Brayer S, Hamimi A, Besnard V, Marchal-Somme J, Ali ZE, Crestani B, Kerdine-Romer S, Boutten A, and Bonay M. Nuclear factor erythroid 2-related factor 2 nuclear translocation induces myofibroblastic dedifferentiation in idiopathic pulmonary fibrosis. *Antioxid Redox Signal* 18: 66–79, 2013.
4. Ashcroft T, Simpson JM, and Timbrell V. Simple method of estimating severity of pulmonary fibrosis on a numerical scale. *J Clin Pathol* 41: 467–470, 1988.
5. Bataller R, Schwabe RF, Choi Y H, Yang L, Paik YH, Lindquist J, Qian T, Schoonhoven R, Hagedorn CH, Lemasters JJ, and Brenner DA. NADPH oxidase signal transduces angiotensin II in hepatic stellate cells and is critical in hepatic fibrosis. *J Clin Invest* 112: 1383–1394, 2003.
6. Bedard K and Krause KH. The NOX family of ROS-generating NADPH oxidases: physiology and pathophysiology. *Physiol Rev* 87: 245–313, 2007.
7. Bocchino M, Agnese S, Fagone E, Svegliati S, Grieco D, Vancheri C, Gabrielli A, Sanduzzi A, and Avvedimento EV. Reactive oxygen species are required for maintenance and differentiation of primary lung fibroblasts in idiopathic pulmonary fibrosis. *PLoS One* 5: e14003, 2010.
8. Brown DI and Griendling KK. Nox proteins in signal transduction. *Free Radic Biol Med* 47: 1239–1253, 2009.
9. Cai GQ, Zheng A, Tang Q, White ES, Chou CF, Gladson CL, Olman MA, and Ding Q. Downregulation of FAK-related non-kinase mediates the migratory phenotype of human fibrotic lung fibroblast. *Exp Cell Res* 316: 1600–1609, 2010.
10. Carnesecchi S, Deffert C, Donati Y, Basset O, Hinz B, Preynat-Seauve O, Guichard C, Arbiser JL, Banfi B, Pache JC, Barazzone-Argiroffo C, and Krause KH. A key role for NOX4 in epithelial cell death during development of lung fibrosis. *Antioxid Redox Signal* 15: 607–619, 2011.
11. Chen J, Xiao X, Chen S, Zhang C, Chen J, Yi D, Shenoy V, Raizada MK, Zhao B, and Chen Y. Angiotensin-converting enzyme 2 priming enhances the function of endothelial progenitor cells and their therapeutic efficacy. *Hypertension* 61: 681–689, 2013.
12. Cook KL, Metheny-Barlow LJ, Tallant EA, and Gallagher PE. Angiotensin-(1–7) reduces fibrosis in orthotopic breast tumors. *Cancer Res* 70: 8319–8328, 2010.
13. Giani JF, Gironacci MM, Munoz MC, Turyn D, and Dominici FP. Angiotensin-(1–7) has a dual role on growth-promoting signalling pathways in rat heart *in vivo* by stimulating STAT3 and STAT5a/b phosphorylation and inhibiting angiotensin II-stimulated ERK1/2 and Rho kinase activity. *Exp Physiol* 93: 570–578, 2008.
14. Goldstein RH and Fine A. Fibrotic reactions in the lung: the activation of the lung fibroblast. *Exp Lung Res* 11: 245–261, 1986.
15. Hagiwara SI, Ishii Y, and Kitamura S. Aerosolized administration of N-acetylcysteine attenuates lung fibrosis induced by bleomycin in mice. *Am J Respir Crit Care Med* 162: 225–231, 2000.
16. Hecker L, Cheng J, and Thannickal VJ. Targeting NOX enzymes in pulmonary fibrosis. *Cell Mol Life Sci* 69: 2365–2371, 2012.

17. Hecker L, Vittal R, Jones T, Jagirdar R, Luckhardt TR, Horowitz JC, Pennathur S, Martinez FJ, and Thannickal VJ. NADPH oxidase-4 mediates myofibroblast activation and fibrogenic responses to lung injury. *Nat Med* 15: 1077–1081, 2009.
18. Hsu HH, Hoffmann S, Endlich N, Velic A, Schwab A, Weide T, Schlatter E, and Pavenstadt H. Mechanisms of angiotensin II signaling on cytoskeleton of podocytes. *J Mol Med (Berl)* 86: 1379–1394, 2008.
19. Jiang T, Gao L, Shi J, Lu J, Wang Y, and Zhang Y. Angiotensin-(1–7) modulates renin-angiotensin system associated with reducing oxidative stress and attenuating neuronal apoptosis in the brain of hypertensive rats. *Pharmacol Res* 67: 84–93, 2013.
20. Kliment CR and Oury TD. Oxidative stress, extracellular matrix targets, and idiopathic pulmonary fibrosis. *Free Radic Biol Med* 49: 707–717, 2010.
21. Kondrikov D, Caldwell RB, Dong Z, and Su Y. Reactive oxygen species-dependent RhoA activation mediates collagen synthesis in hyperoxic lung fibrosis. *Free Radic Biol Med* 50: 1689–1698, 2011.
22. Konigshoff M, Wilhelm A, Jahn A, Sedding D, Amarie OV, Eul B, Seeger W, Fink L, Gunther A, Eickelberg O, and Rose F. The angiotensin II receptor 2 is expressed and mediates angiotensin II signaling in lung fibrosis. *Am J Respir Cell Mol Biol* 37: 640–650, 2007.
23. Kostenis E, Milligan G, Christopoulos A, Sanchez-Ferrer CF, Heringer-Walther S, Sexton PM, Gembardt F, Kellett E, Martini L, Vanderheyden P, Schultheiss HP, and Walther T. G-protein-coupled receptor Mas is a physiological antagonist of the angiotensin II type 1 receptor. *Circulation* 111: 1806–1813, 2005.
24. Lambeth JD. NOX enzymes and the biology of reactive oxygen. *Nat Rev Immunol* 4: 181–189, 2004.
25. Lang YD, Hung CL, Wu TY, Wang LF, and Chen CM. The renin-angiotensin system mediates hyperoxia-induced collagen production in human lung fibroblast. *Free Radic Biol Med* 49: 88–95, 2010.
26. Lyle AN, Deshpande NN, Taniyama Y, Seidel-Rogol B, Pounkova L, Du P, Papaharalambus C, Lassegue B, and Griendling KK. Poldip2, a novel regulator of Nox4 and cytoskeletal integrity in vascular smooth muscle cells. *Circ Res* 105: 249–259, 2009.
27. Manoury B, Nenan S, Leclerc O, Guenon I, Boichot E, Planquois JM, Bertrand CP, and Lagente V. The absence of reactive oxygen species production protects mice against bleomycin-induced pulmonary fibrosis. *Respir Res* 6: 11, 2005.
28. Marshall RP, Gohlke P, Chambers RC, Howell DC, Bottoms SE, Unger T, McAnulty RJ, and Laurent GJ. Angiotensin II and the fibroproliferative response to acute lung injury. *Am J Physiol Lung Cell Mol Physiol* 286: L156–L164, 2004.
29. Martyn KD, Frederick LM, von Loehneysen K, Dinauer MC, and Knaus UG. Functional analysis of Nox4 reveals unique characteristics compared to other NADPH oxidases. *Cell Signal* 18: 69–82, 2006.
30. Meng Y, Yu CH, Li W, Li T, Luo W, Huang S, Wu PS, Cai SX, and Li X. Angiotensin-converting enzyme 2/angiotensin-(1–7)/Mas axis protects against lung fibrosis by inhibiting the MAPK/NF-κB pathway. *Am J Respir Cell Mol Biol* 50: 723–736, 2014.
31. Montezano AC, Callera GE, Yogi A, He Y, Tostes RC, He G, Schiffrin EL, and Touyz RM. Aldosterone and angiotensin II synergistically stimulate migration in vascular smooth muscle cells through c-Src-regulated redox-sensitive RhoA pathways. *Arterioscler Thromb Vasc Biol* 28: 1511–1518, 2008.
32. Moon JY, Tanimoto M, Gohda T, Hagiwara S, Yamazaki T, Ohara I, Murakoshi M, Aoki T, Ishikawa Y, Lee SH, Jeong KH, Lee TW, Ihm CG, Lim SJ, and Tomino Y. Attenuating effect of angiotensin-(1–7) on angiotensin II-mediated NAD(P)H oxidase activation in type 2 diabetic nephropathy of KK-AyTa mice. *Am J Physiol Renal Physiol* 6: F1271–F1282, 2011.
33. Ni J, Dong Z, Han W, Kondrikov D, and Su Y. The role of RhoA and cytoskeleton in myofibroblast transformation in hyperoxic lung fibrosis. *Free Radic Biol Med* 61C: 26–39, 2013.
34. Ni L, Feng Y, Wan H, Ma Q, Fan L, Qian Y, Li Q, Xiang Y, and Gao B. Angiotensin-(1–7) inhibits the migration and invasion of A549 human lung adenocarcinoma cells through inactivation of the PI3K/Akt and MAPK signaling pathways. *Oncol Rep* 27: 783–790, 2012.
35. Nlandu KS, Dizin E, Sossauer G, Szanto I, Martin PY, Feraille E, Krause KH, and de Seigneux S. NADPH-oxidase 4 protects against kidney fibrosis during chronic renal injury. *J Am Soc Nephrol* 23: 1967–1976, 2012.
36. Otsuka M, Takahashi H, Shiratori M, Chiba H, and Abe S. Reduction of bleomycin induced lung fibrosis by candesartan cilexetil, an angiotensin II type 1 receptor antagonist. *Thorax* 59: 31–38, 2004.
37. Park S, Ahn JY, Lim MJ, Kim MH, Yun YS, Jeong G, and Song JY. Sustained expression of NADPH oxidase 4 by p38 MAPK-Akt signaling potentiates radiation-induced differentiation of lung fibroblast. *J Mol Med (Berl)* 88: 807–816, 2010.
38. Rey-Parra GJ, Vadivel A, Coltan L, Hall A, Eaton F, Schuster M, Loibner H, Penninger JM, Kassiri Z, Oudit GY, and Thebaud B. Angiotensin converting enzyme 2 abrogates bleomycin-induced lung injury. *J Mol Med (Berl)* 90: 637–647, 2012.
39. Serrander L, Cartier L, Bedard K, Banfi B, Lardy B, Plastre O, Sienkiewicz A, Forro L, Schlegel W, and Krause KH. NOX4 activity is determined by mRNA levels and reveals a unique pattern of ROS generation. *Biochem J* 406: 105–114, 2007.
40. Serrano-Mollar A, Closa D, Prats N, Blesa S, Martinez-Losa M, Cortijo J, Estrela JM, Morcillo EJ, and Bulbena O. *In vivo* antioxidant treatment protects against bleomycin-induced lung damage in rats. *Br J Pharmacol* 138: 1037–1048, 2003.
41. Shenoy V, Ferreira AJ, Qi Y, Fraga-Silva RA, Díez-Freire C, Dooies A, Jun JY, Sriramula S, Mariappan N, Pourang D, Venugopal CS, Francis J, Reudelhuber T, Santos RA, Patel JM, Raizada MK, and Katovich MJ. The angiotensin-converting enzyme 2/angiogenesis-(1–7)/Mas axis confers cardiopulmonary protectionagainst lung fibrosis and pulmonary hypertension. *Am J Respir Crit Care Med* 182: 1065–1072, 2010.
42. Shinohara M, Shang WH, Kubodera M, Harada S, Mitsushita J, Kato M, Miyazaki H, Sumimoto H, and Kamata T. Nox1 redox signaling mediates oncogenic Ras-induced disruption of stress fibers and focal adhesions by down-regulating Rho. *J Biol Chem* 282: 17640–17648, 2007.
43. Suganuma H, Sato A, Tamura R, and Chida K. Enhaced migration of fibroblasts derived from lungs with fibrotic lesions. *Thorax* 50: 984–989, 1995.

44. Takahashi F, Takahashi K, Okazaki T, Maeda K, Ienaga H, Maeda M, Kon S, Uede T, and Fukuchi Y. Role of osteopontin in the pathogenesis of bleomycin-induced pulmonary fibrosis. *Am J Respir Cell Mol Biol* 24: 264–271, 2001.
45. Thomas J, Gross MD, Gary W, and Hunningchake MD. Idiopathic pulmonary fibrosis. *N Engl J Med* 345: 517–525, 2001.
46. Tufvesson E and Westergren-Thorsson G. Biglycan and decorin induce morphological and cytoskeletal changes involving signalling by the small GTPases RhoA and Rac1 resulting in lung fibroblast migration. *J Cell Sci* 116: 4857–4864, 2003.
47. Ushio-Fukai M, Hilenski L, Santanam N, Becker PL, Ma Y, Griendling KK, and Alexander RW. Cholesterol depletion inhibits epidermal growth factor receptor transactivation by angiotensin II in vascular smooth muscle cells: role of cholesterol-rich microdomains and focal adhesions in angiotensin II signaling. *J Biol Chem* 276: 48269–48275, 2001.
48. White ES, Thannickal VJ, Carskadon SL, Dickie EG, Livant DL, Markwart S, Toews GB, and Arenberg DA. Integrin $\alpha 4\beta 1$ regulates migration across basement membranes by lung fibroblasts: a role for phosphatase and tensin homologue deleted on chromosome 10. *Am J Respir Crit Care Med* 168: 436–442, 2003.
49. Wingler K, Wunsch S, Kreutz R, Rothermund L, Paul M, and Schmidt HH. Upregulation of the vascular NAD(P)H-oxidase isoforms Nox1 and Nox4 by the renin-angiotensin system *in vitro* and *in vivo*. *Free Radic Biol Med* 31: 1456–1464, 2001.
50. Wu RF, Ma Z, Myers DP, and Terada LS. HIV-1 Tat activates dual Nox pathways leading to independent activation of ERK and JNK MAP kinases. *J Biol Chem* 282: 37412–37419, 2007.
51. Xia H, Suda S, Bindom S, Feng Y, Gurley SB, Seth D, Navar LG, and Lazartigues E. ACE2-mediated reduction of oxidative stress in the central nervous system is associated with improvement of autonomic function. *PLoS One* 6: e22682, 2011.
52. Yamagishi S, Nakamura K, Ueda S, Kato S, and Imaizumi T. Pigment epithelium-derived factor (PEDF) blocks angiotensin II signaling in endothelial cells via suppression of NADPH oxidase: a novel anti-oxidative mechanism of PEDF. *Cell Tissue Res* 320: 437–445, 2005.
53. Yang J, Tan Y, Zhao F, Ma Z, Wang Y, Zheng S, Epstein PN, Yu J, Yin X, Zheng Y, Li X, Miao L, and Cai L. Angiotensin II plays a critical role in diabetic pulmonary fibrosis most likely via activation of NADPH oxidase-mediated nitrosative damage. *Am J Physiol Endocrinol Metab* 301: E132–E144, 2011.
54. Zhang C, Zhao YX, Zhang YH, Zhu L, Deng BP, Zhou ZL, Li SY, Lu XT, Song LL, Lei XM, Tang WB, Wang N, Pan CM, Song HD, Liu CX, Dong B, Zhang Y, and Cao Y. Angiotensin-converting enzyme 2 attenuates atherosclerotic lesions by targeting vascular cells. *Proc Natl Acad Sci U S A* 107: 15886–15891, 2010.
55. Zhang F, Hu Y, Xu Q, and Ye S. Different effects of angiotensin II and angiotensin-(1–7) on vascular smooth muscle cell proliferation and migration. *PLoS One* 5: e12323, 2010.
56. Zhang R, Wu Y, Zhao M, Liu C, Zhou L, Shen S, Liao S, Yang K, Li Q, and Wan H. Role of HIF-1alpha in the regulation ACE and ACE2 expression in hypoxic human pulmonary artery smooth muscle cells. *Am J Physiol Lung Cell Mol Physiol* 297: L631–L640, 2009.
57. Zhao W, Chen SS, Chen Y, Ahokas RA, and Sun Y. Kidney fibrosis in hypertensive rats: role of oxidative stress. *Am J Nephrol* 28: 548–554, 2008.
58. Zhao W, Zhao T, Chen Y, Ahokas RA, and Sun Y. Oxidative stress mediates cardiac fibrosis by enhancing transforming growth factor-beta1 in hypertensive rats. *Mol Cell Biochem* 317: 43–50, 2008.
59. Zhong J, Basu R, Guo D, Chow FL, Byrns S, Schuster M, Loibner H, Wang XH, Penninger JM, Kassiri Z, and Oudit GY. Angiotensin-converting enzyme 2 suppresses pathological hypertrophy, myocardial fibrosis, and cardiac dysfunction. *Circulation* 122: 717–728, 2010.

Address correspondence to:
Dr. Xu Li
Department of Hepatology
Nanfang Hospital
The Southern Medical University
Guangzhou 510515
China

E-mail: mylx99@163.com

Date of first submission to ARS Central, December 30, 2013; date of final revised submission, July 15, 2014; date of acceptance, August 4, 2014.

Abbreviations Used

α-sma = α-smooth actin
ACE = angiotensin-converting enzyme
ACE2 = angiotensin-converting enzyme 2
Ang(1–7) = angiotensin (1–7)
AngII = angiotensinII
AT1R = angiotensinII type 1 receptor
BLM = bleomycin
CTGF = connective tissue growth factor
DCF-DA = 2,7-dichlorofluorescein diacetate
DMEM = Dulbecco's modified Eagle's medium
DPI = diphenylene iodonium
ECM = extracellular matrix
GST = glutathione S-transferase
H_2O_2 = hydrogen peroxide
IP = immunoprecipitation
IPF = idiopathic pulmonary fibrosis
lentiACE2 = lentivirus-mediated ACE2
NAC = *N*-acetylcysteine
NOX = NADPH oxidases
NOX4 = NADPH oxidase-4
PBS = phosphate-buffered saline
PDGF = platelet-derived growth factor
RT-PCR = reverse transcription polymerase chain reaction
RAS = renin-angiotensin system
Rock = Rho kinase
ROS = reactive oxygen species
siRNA = small-interfering RNA
TGFβ = transforming growth factor β
VSMCs = vascular smooth muscle cells